DEVELOPMENT AND TESTING OF LIQUID TO SOLID

SCINTILLATING NEUTRON DETECTORS

A Thesis
Presented to
The Academic Faculty

by

William Michael Meier

In Partial Fulfillment
of the Requirements for the Degree
Masters of Science in Nuclear Engineering in the
Woodruff School of Mechanical Engineering

Georgia Institute of Technology
May 2016

DEVELOPMENT AND TESTING OF LIQUID TO SOLID

SCINTILLATING NEUTRON DETECTORS

Approved by:

Dr. Anna Erickson, Advisor
School of Mechanical Engineering
Nuclear Engineering Program
Georgia Institute of Technology

Dr. Nolan E. Hertel
School of Mechanical Engineering
Nuclear Engineering Program
Georgia Institute of Technology

Dr. Antonia Antoniou
School of Mechanical Engineering
Mechanical Engineering Program
Georgia Institute of Technology

Date Approved: 19 April 2016

ACKNOWLEDGEMENTS

TABLE OF CONTENTS

LIST OF TABLES

LIST OF FIGURES

LIST OF EQUATIONS

LIST OF ABBREVIATIONS

LS	Liquid Scintillation
SNM	Special Nuclear Materials
PSD	Pulse Shaped Discrimination
PVT	Polyvinyl toluene
FOM	Figure of Merit
PPO	Diphenyl oxazole
POPOP	5-Phenyl-2-[4-(5-phenyl-1,3-oxazol-2-yl)phenyl]-1,3-Oxazole
PDMS	Polydimethylsiloxane
LENA	Low Energy Neutrino Astronomy
LAB	Linear Alkyl Benzene
PMP	Phenyl-Mesityle-Pyrazolin
MSB	Bis-Methylstyryl-Benzene
Li-3-PSA	Phenyl salicylic Acid
PMT	Photomultiplier Tube
PTFE	Polytetrafluoroethylene
RSEL	Radiological Science and Engineering Laboratory
PAA	Polyacrylic Acid
Q_{long}	Total Charge Collected by the Digitzer
Q_{short}	Collected Charge in Short Gate
FWHM	Full-Width-Half-Max
E'	Energy of Compton Edge
E_o	Gamma Ray Energy

SUMMARY

The purpose of this research is to determine the feasibility of creating an affordable and durable neutron detector for usage in the field surveys, site inspections, and transportation hub monitoring. Currently, organic scintillating detectors are an established method of detecting neutrons but are either costly, fragile solids like stilbene, or flammable liquids like benzene. In this work, several scintillation mixtures were tested with a PuBe source, which emits both neutrons and gamma rays. The pulse shape discrimination method was utilized to separate the signal pulses created from the mixed radiation field of the PuBe source. Two candidate mixtures were selected for solidification with elastomers for their verified neutron detection capabilities. The solid detectors measured high energy neutrons and gamma rays from the PuBe source. The solidified detectors have a Figure of Merit for separating neutrons of 0.859 ±0.419 and cost $0.13 per gram, while commercially available stilbene separates neutrons from gammas with a Figure of Merit of 4.70 and costs $64.36 per gram. This research shows that it is feasible to create affordable solid organic scintillators sensitive to high energy neutrons.

CHAPTER 1

INTRODUCTION

Background

In today's world, nuclear power negotiations are a reoccurring but serious dispute between nations. One of the reasons negotiations are necessary and prudent is to prevent the proliferation of Special Nuclear Materials (SNM). SNM are the isotopes uranium-233, uranium-235, and all plutonium isotopes due to their usage in nuclear weapons production.[1] The availability of SNM is a matter of national security and safety because of the potential for mass destruction if it is abused. One manner of preventing the proliferation of SNM is the employment of robust, versatile, and mobile inspection equipment.

On August 30th, 2015, the U.S. Energy Secretary Ernest Moniz gave a speech at the University of Colorado calling for continued research and development of SNM detectors in order to "form the basis of a new era for nonproliferation verification."[2] Secretary Moniz argued that nuclear inspections are an effective deterrence against covert pathways to a nuclear bomb by verifying the safe handling and secure storage of SNM. He argued that accurate and precise radiation detectors will improve the tracking and quantifying of SNM during the nuclear fuel cycle and prevent diversion for illicit purposes. Additionally, the U.S. Department of Energy's 2014 Strategic Plan lists their second goal, of three, as "Nuclear Security" with the stated objectives of "strengthen key science, technology, and engineering capabilities and modernize the national security infrastructure" and "reduce global nuclear security threats."[2] Thus, developing detectors and systems for nuclear inspections are essential for promoting nuclear power transparency and meeting the goals of the DoE by ushering in a new era of nonproliferation.

One type of detector that could provide a robust, versatile, and mobile system is a liquid scintillation (LS) detector. LS detectors provide inspectors with a versatile system because various mixtures can be utilized and replaced in order to choose the optimal mixture for their mission. LS detectors are potent gamma ray and neutron detectors and commonly utilized for neutrino observatories.[3] Unfortunately, LS mixtures are not durable and need to be stored away from sources of heat in inert containers, due to their solvent and flammable properties. The low vapor points, a flammable property, of LS detectors cause the mixtures to evaporate quickly when not contained properly.

Similarly, a solid organic scintillation detector may provide effective, versatile detection systems. Solid organic or plastic detectors have been utilized as effective thermal and fast neutron detectors since the 1990s, because they do not spill if mishandled and are less flammable compared to liquid detectors.[4] The disadvantages of solid organic detectors are general brittleness, thermal gradient cracking, and cost. A 1 cm x 1 cm x 8 cm prism of scintillating plastic can cost as much as $500, or $62.50 per cm^3. If an effective, cheap solid plastic detector can be developed that is not brittle or sensitive to temperatures, then a viable solid detector can meet the stated goals of the DoE.

Motivation

In this work, new solid neutron detectors were developed in an attempt to create affordable detectors and accomplish the security goals of Secretary Moniz. More cost efficient neutron detectors are desired because Helium-3 detectors are becoming more expensive. The rising cost of He-3 is important because He-3 neutron detectors are considered one of the most advantageous neutron detectors because their neutron-proton reaction has a higher cross section than that of neutron capture by boron and other isotopes.[4] In a 2014 study, one metric ton of He-3 was valued to be $3.7 billion.[5] The cost of He-3 is increasing because the most common source of He-3 is from dismantling

warheads, and fewer and fewer nuclear warheads are being dismantled.[6] Due to this high cost, researchers have continued experimenting with ways to create inexpensive alternatives to He-3 detectors.

Current areas of alternative detectors are LS detectors, stilbene crystal detectors, hybrid detectors, and solidified LS mixtures. The innovative solidified LS detectors have inspired this thesis by attempting to create new solid detectors by mixing a liquid scintillator with a solidifying agent. The new solid detectors made during this project are an attempt to make affordable, effective, and field-capable detectors. If successful, these detectors may provide a method of easily detecting covert nuclear programs and degrading the risk of SNM proliferation.

Prior and Current Approaches to Neutron Detection

Significant neutron radiation detection experiments began in 1940 when Barshall and Kanner studied the energy distribution of scattered neutrons. By colliding neutrons with a hydrogen target, they were able to demonstrate that neutrons, below 10 MeV, have isotropic scattering, in a center of mass system, and that the energy distribution of recoil protons is uniform from 0 to the neutron's kinetic energy.[7] The significance of the recoil energy distribution discovery is that (n,p) scattering, or elastic scattering, can transfer the maximum amount of energy to the nucleus at the same probability of any other fraction of the neutron's energy.

Building upon the studies of elastic scattering in organic solvents, Kallman and Furst proved that organic liquid solutions were feasible for neutron radiation detection by increasing the concentration of their solvent. In 1950, they conducted an experiment in which a beaker was filled with different organic solutions, sealed, and exposed to various radiation sources. They were able to demonstrate that organic solvents were transferring energy to fluorescent dopants dissolved in the solvent and that the concentration of fluors were directly related to light output.[7]

In 1964, two groups of scientists constructed He-3 proportional counters in order to improve spectroscopy and detection of fast neutrons. Like other proportional counters, the He-3 proportional counter is filled with He-3 and an inert gas where incident neutrons create hydrogen ions and a charge is built inside the gas chamber for collection and analysis.[4] When a neutron interacts with a He-3 nucleus there is a relatively large chance of producing a tritium molecule and a free proton.[4] The Q value of the He-3 (n,p) reaction is 0.764 MeV.[4] The following reaction equation demonstrates this:

$$_2^3He + {}_0^1n \rightarrow {}_1^3H + {}_1^1p \quad Q = 0.764 \; MeV \qquad \text{Equation 1}$$
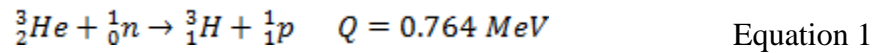
The He-3 (n,p) reaction enables a He-3 proportional counter to collect the kinetic energy of the reaction products.[4]
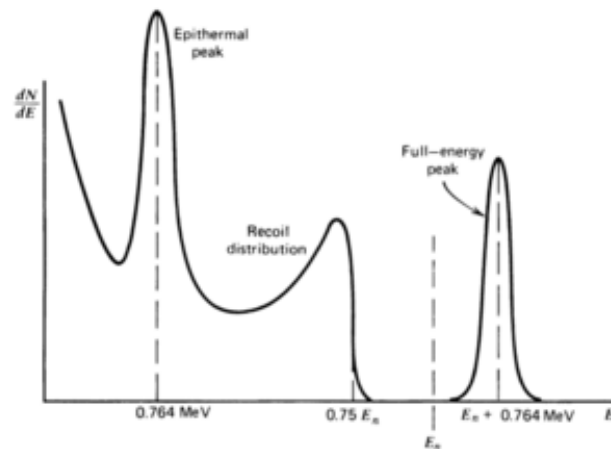
Figure 1. Differential energy spectrum from fast neutrons on a He-3 detector.[4]

The effectiveness of the He-3 (n,p) reaction, shown in Figure 1, compelled the He-3 detectors to be accepted as the reliable He-3 neutron detector.[4]

The ability of solid organic detectors to detect neutrons through scintillation was observed as early as 1962, but methods to begin discriminating between scintillations caused neutron and gamma rays did not start being used until the 1990s.[4] The most common method has come to be known as Pulse Shape Discrimination (PSD), in which the differences in rise and fall times of scintillation pulses are analyzed. Because gamma rays induce scintillation by fast electron generation and neutrons cause scintillation by recoiling protons, their respective scintillation pulses have different timing characteristics.[4] In stilbene, gamma ray pulses have a larger fraction of light in their prompt component as compared to recoil protons caused by neutrons.[4] Using PSD, organic scintillators can become more useful neutron detectors.

One particular area of interest in current organic scintillation is the transformation of effective liquid scintillators into solid neutron detectors. At Lawrence Livermore National Laboratory, many liquid organic scintillators with dopants were mixed into a polyvinyl toluene (PVT) matrix to create solid detectors.[8] The mixtures were prepared in nitrogen filled containers, removing the oxygen, and mixed to various weight percentages with the PVT matrix.[8] After mixing, the mixtures were poured into glass containers and placed into an oven for curing. Once solid, the glass container was broken to retrieve the solid scintillators. The Figure of Merit (FOM), a measure of the separation of neutron and gamma ray curves, of the solidified detectors was determined and compared to the commercially available neutron detectors EJ-301, a liquid, and stilbene.
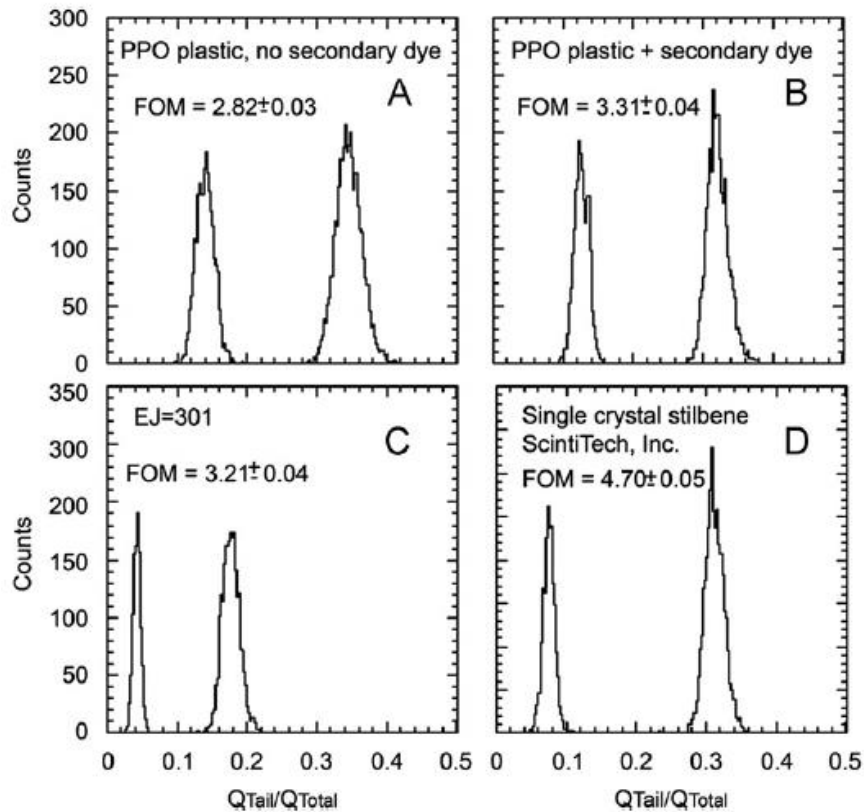
Figure 2. Scintillator FOM Comparison of two solidified LS mixtures in PVT, EJ 301, and Stilbene.[8]

The results in Fig. 2 demonstrate that one of the produced solid scintillators had a greater FOM than EJ 301, but not larger than stilbene. These results are promising because these "liquid-to-solid" scintillators are more effective than some liquids and cheaper than solid stilbene.

Another research group at the Laboratoie Capteurs et Architectures Électroniques, (CEA), has successfully created solids from liquid scintillation mixtures. They have been able to create solids that are 28.6% scintillator by weight with a FOM of approximately 1.[9] These solid detectors were made by mixing styrene and vinyl toluene monomers with 5-Phenyl-2-[4-(5-phenyl-1,3-oxazol-2-yl)phenyl]-1,3-oxazole (POPOP) and diphenyl oxazole (PPO) in an argon-filled environment.[9] Dr. Zaitseva's and CEA's research into

6

manufacturing affordable, durable, and effective solid neutron detectors are the inspiration for this work.

Thesis Objectives

The objective of the research is to experimentally fabricate an effective liquid scintillator mixture, to develop it into a solidified detector, and characterize the neutron detection capabilities of the detector. Affordable solid detectors can meet the security demands in future nuclear power program inspections to identify covert diversions of fissile material. If the research is successful, a prototype solidified detector will demonstrate the feasibility of fissile material in a mixed radiation field from nuclear power reactors or nuclear fuel storage facilities.

CHAPTER 2

THEORY

Gamma Ray Properties and Interactions

Gamma rays are powerful photons that are not visible to the naked eye, but contain enough energy to free electrons from the orbits of atoms, or ionize atoms. Gamma rays are created through positron-electron annihilation, de-excitation of nuclei, or nuclear reactions. All annihilation gamma rays have an energy of 0.511 MeV. The gamma rays emit during de-excitation of nuclei and defined energies as the nucleus transitions to a lower energy state.[4] Unlike positron annihilation, the energies of de-excitation gamma ray are various and dependent upon the transition the nuclei. Similar to nuclear de-excitation, gamma rays emitted from nuclear reactions are characteristic to their reaction and of a much higher energy. C-13 emits a 6.130 MeV gamma ray when it absorbs an alpha particle.[4] These characteristic gamma rays are significant because they are used to identify the radioactive material which emitted it.

Gamma rays interact with matter through three major mechanisms: photo-electric absorption, Compton scattering, and pair production. The probability of how an incident gamma ray will interact in matter with is dependent upon the size of the nucleus, Z or number of nucleons, and the energy of the gamma ray.
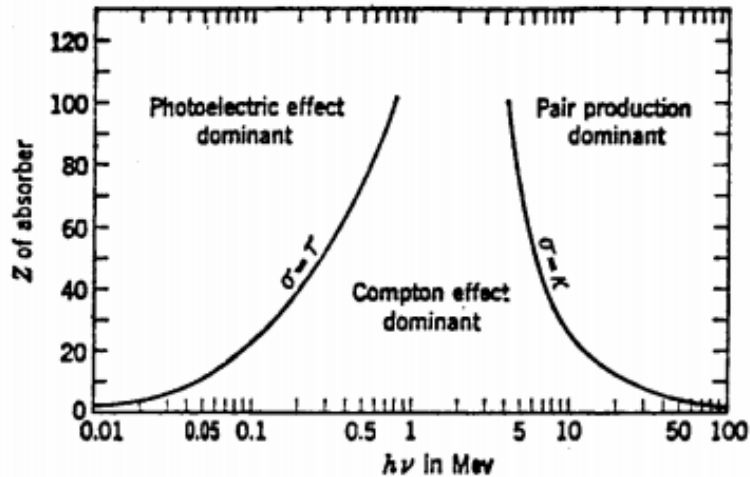
Figure 3. Relative importance diagram of the three major types of gamma ray interaction.[4]

Figure 3 shows that low Z materials are dominated by the Compton effect and that moderate and high Z materials experiences all three mechanisms. In most materials, the dominant interacting mechanism goes from photoelectric, Compton scattering, to pair production as the gamma ray energy is increased.

Photoelectric absorption is a process that results in the ejection of an electron from an atom's electron cloud. In this process, the energy of gamma ray is transferred to the ejected electron, minus the electron's binding energy, and the gamma ray is absorbed.[4] After the electron is expelled, the remaining atom is ionized and has a hole in one of its electron shells. The hole is filled quickly by the surrounding medium and the electron rearrangement emits one or more characteristic x-rays photons.[4] The characteristic x-rays are generally absorbed near their emission site, but can interfere with detectors if they escape.[4] While the photo-electric effect is dominant with low energy gamma rays, gamma rays begin to interact through Compton scattering within the range of 0.5 to 5 MeV.

Compton scattering is a process in which the incident photon interacts with an atom's electron, unlike the photo-electric effect. In Compton scattering, the incident photon interacts with a loosely bound electron, which is considered free, creating a recoil electron and a scattered photon. The incident photon is deflected, or scattered, by an electron through an angle and the gamma ray transfers a portion of its energy to the electron, which recoils it out of the atom.[4] The third major mechanism of gamma rays interacting with matter is pair production.

If a gamma ray's energy exceeds 1.02 MeV, or twice the rest-mass energy of an electron, the gamma ray has met the energy threshold for this pair production. In pair production, the gamma ray interacts with the atom's nucleus and is converted into a positron and an electron of equal kinetic energies, minus the 1.02 MeV threshold.[4] The electron will travel until it is absorbed by another atom. The positron will travel until it is slowed enough by the absorbing medium for positron annihilation. The positron will annihilate itself with an absorbing electron and create two distinct gamma rays of 0.511 MeV.[7]

Gamma Ray Detection Theory

In organic scintillators, gamma rays are detected by their energy deposition into matter. The matter of the organic scintillator is excited by gamma rays through the mechanisms of photo-electric absorption, Compton scattering, and pair production. Each of these events ionize and excite the material, and eventually leads the scintillator to convert the energy of these events into fluorescence emission.[7] The charged particles produced by the gamma ray interactions impart their kinetic energy into the surrounding organic molecules' electron clouds and nucleus as they pass nearby and eventually stop.[4] The absorbed kinetic energy is transformed by the molecules into vibrational energy and its electrons enter into higher energy states. In order to de-excite, fluorescence emission

occurs in the organic molecule, instead of within the crystalline lattice of inorganics like sodium iodide.[4]

Organic molecules respond to incident radiation different than inorganics due to the unique structure of the carbon, C, atom. Organic molecules contain double C to C bonds, or π-bonds, and form molecular rings, shown by Fig. 4. Benzene, C_6H_6, is a common organic scintillator because it can contain 3 π-bonds.
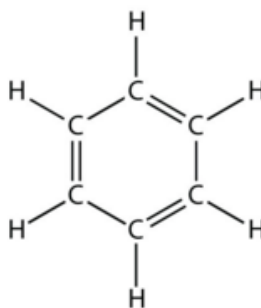
Figure 4. Benzene ring molecule diagram with 3 π-bonds.[10]

Π-electrons are significant for scintillation because they are treated as orbitals of free electrons around the molecular perimeter. Their unique orbit creates a plethora of discrete energy levels that are dependent upon the molecular perimeter, the electron spin, and the orbital quantum number.[7] These energy levels are called π-energy states and are spaced 0.16 eV apart and are shown in Fig. 5.
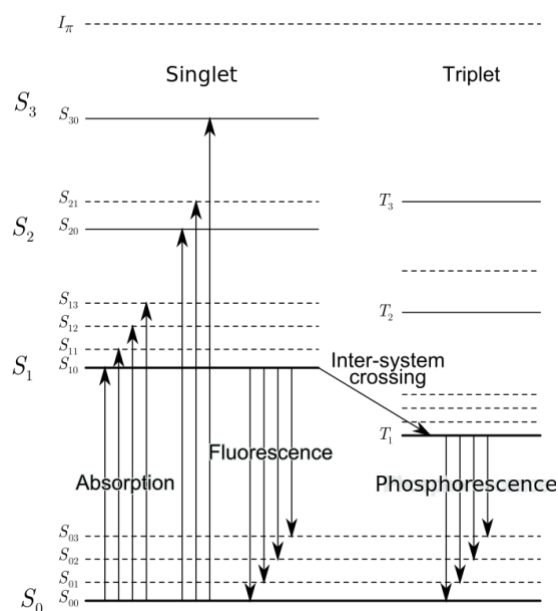
Figure 5. Π-electron energy levels of an organic molecule.[7]

Benzene creates discrete detectable light as the molecule transitions from high π-energy states to lower states.[7]

The electrons emit light either by the processes of fluorescence or phosphorescence. Fluorescence is the prompt process of light emission as an organic molecule transitions down from an excited state to the one the ground vibrational states.[4] Phosphorescence occurs in organic molecules if the molecule changes into a triplet state through a process called the inter-system crossing and then decays to the ground states.[4] Fluorescence in organic molecules occurs on the nanosecond scale and delayed phosphorescence occurs on the millisecond scale.[4]

An important characteristic of organic scintillators is the absorption and quenching of scintillation occurring within the medium. Organic scintillators absorb a portion of the light they emit because there is an overlap in the wavelength spectrum of light that they absorb and emit. This overlap is called the "Stokes Shift."[4] Quenching is the de-excitation of organic molecules through "lightless" processes which degrade by

heat and not fluourescence.[4] To counter quenching and the Stokes Shift, wavelength shifters are included in organic scintillators. Wavelength shifters assist the fluor by "shifting" the light emitted by the primary scintillator to a longer wavelength that will not be absorbed and reducing the occurrence of quenching.[4]

Neutron Properties and Interactions

Neutrons being energetically ejected from a nucleus are a unique radioactive decay signature of fissile isotopes, like SNM, and fission products. Organic scintillators are occasionally referred to as proton recoil scintillators when used to detect neutrons.. They are called proton recoil detectors because it is through neutrons recoiling protons, which cause the scintillations as they deposit energy in the surrounding medium. Unlike gamma rays which mainly interact with electrons, neutrons are more likely to interact with the nucleus. Neutrons interacting with hydrogen are of particular interest because neutrons have the same probability of scattering at 0 degrees as 90 degrees off of hydrogen atoms and can impart their full energy into the proton.[7]   Since organic materials contain multiple atoms of hydrogen for each molecule, like benzene, the probability to detect neutrons is increased.   Another important property of neutron-proton collisions is that the probability of transferring any fraction or all of the neutron energy into the recoil proton is the same. Thus, the energy distribution of recoil protons is the same from 0 MeV to the energy of the neutron.[7] By measuring the energy spectrum of incident neutrons the average energy of emitted neutrons can be determined.

Neutrons interact with matter by inelastic scattering, fission, and absorption. When a neutron inelastically scatters with a recoil nuclei, the transferred energy is not all converted into kinetic energy and the nucleus is elevated to a higher state. In this higher state, the nucleus de-excites by emitting a gamma-ray.[7] When a neutron is absorbed into a nucleus, the mass number of the nucleus increases and produces a stable or unstable isotope. A stable isotope will not have any further reaction, but an unstable isotope will

decay respectively to its characteristics. A common absorption reaction used to detect neutrons is the Li-6(n,α) reaction which has a Q-value of 4.78 MeV.[4] Nuclear fission is when an unstable atom accepts a neutron and immediately splits its nucleus into two or more pieces and releases heat, gamma rays, and neutrons. Fissions most often occur in fissile materials, like U-235, which undergo prompt fission when they absorb a thermal neutron. Some neutron detectors utilize neutron absorption reactions and fission as a means to detect neutrons instead of scattering.

Organic Scintillation Detection Theory

In both liquid and solid organic scintillators, the process of producing detectable light is the same. Both mediums use a solvent or solid material which consists of a high concentration of hydrogen molecules for neutron interactions and electrons for gamma ray interactions. When the solvent and fluor molecules are excited by the moving charged recoil protons or ejected electrons, the molecules de-excite by isotropically emitting light. The wavelength shifters absorb the emitted light and "shift" it to a longer wavelength. Fig. 6 is a visual representation of the process.
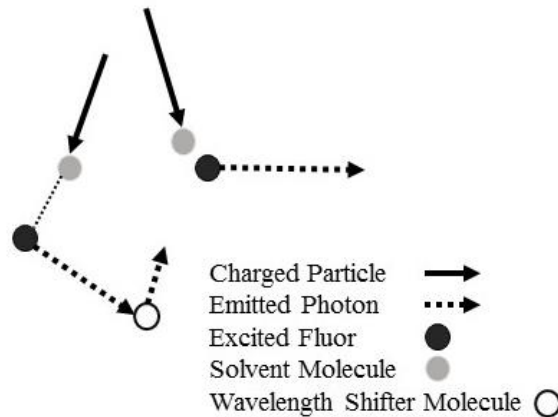
Figure 6. Organic Scintillation diagram.

The components of the plastic and liquid mixture are of extreme importance and have been thoroughly studied, because they determine the probability of radiation interactions and efficiency of the scintillation process.[7] The efficiency of the scintillation process can be affected in many ways, but the most significant one is the concentration of the fluor to the solvent. In 1959, Brown, Furst, and Kallman observed that the efficiency of energy transfer from their solvent, Xylene, to their fluor, PPO was a function of the PPO concentration. The higher the PPO concentration, the higher the energy transfer percentage.[7] Additionally, the determined that once a fluor saturation limit was reached then the transfer percentage decreased, and that impurities like dissolved oxygen quenched their mixture and reduced efficiency.[7] Surfactants are an uncommon additive for organic detectors. Surfactants or emulsifiers, like Triton-X, assist in the dissolving of fluors other additives, but can be detrimental through quenching and reducing scintillation efficiency. If a solution is using a neutron absorbing dopant, like gadolinium, then a surfactant might be used to increase the concentration of the dopants. Gadolinium and other neutron absorbers are used in both liquid and solid organic detectors due to their significant neutron absorption cross section. With an absorption dopant, an exact signal can used to detect neutrons being absorbed instead of neutrons interacting with a scintillator.

An important characteristic of radiation detectors is the linear dependence upon the energy of the charged particle moving within the detector and the light output.[4] Linear dependence of light output is essential for analyzing the energy of neutrons and gamma rays through spectroscopy. Due to deposited energy linear dependence, organic scintillators form count peaks of light intensity when exposed to gamma rays of distinct energy and count shoulders when mono-energetic neutrons interact with the scintillator.

Compton scattering of gamma rays within the detector's medium form a shoulder called the Compton edge. The Compton edge's maximum energy is limited by an electron backscattered and the largest amount of energy is transferred to the electron as the gamma ray scatters away.[4] If both the gamma ray and Compton scattered electron are absorbed within the medium, then a full energy count can be collected, but if the gamma ray escapes then a count will occur within the Compton edge.
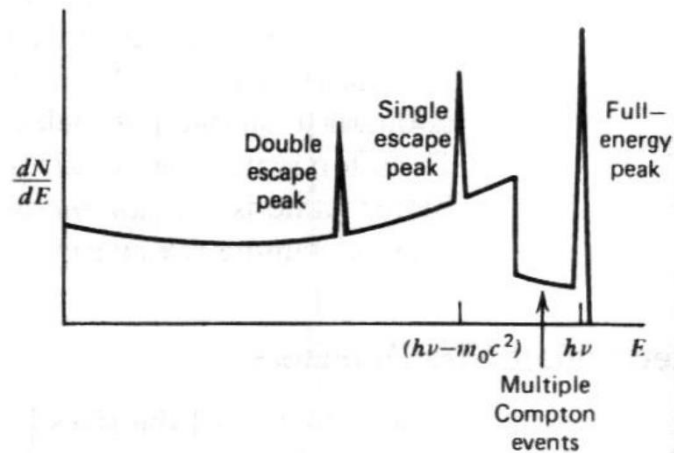
Figure 7. Gamma ray histogram depicting Compton edge and escape peaks.[4]

Figure 7 visually demonstrates how a Compton edge and full energy peak appear with the single and double escape peaks from pair production. Single and double escape peaks are products of pair production in the detecting medium and are a function of whether the two positron annihilation photons absorb or escape.

The ability of organic scintillators to scintillate for neutrons and gamma rays, their fast response, and low Z-value constituents make them candidates to detect the fast neutrons of SNM. The specific properties of organic scintillators that provide an effective means of fast neutron detection are:[4]

1. The high hydrogen content which has a hydrogen to carbon ratio greater than one.

2. Organic scintillators that produce at least 50 percent of the light output of the organic crystal anthracene.

3. The wavelength of emission is detectable in the range of the visible and ultra-violet wavelength spectral response, between 300-500 nm.

4. The medium's transparency to the wavelength of its own emission, with or without wavelength shifters to minimize optical absorption, and an acceptable index of refraction near glass (~1.5).

5. The conversion of deposited energy to light output is linear and proportional.

6. The decay time of the scintillations should be short to enable fast signal pulse generation.

Pulse Shape Discrimination Theory

Organic scintillators exhibit varying intensities of fast and slow components of light yield according to the mass and energy of incident particles. These different components are dependent upon the specific ionizations of the particle. Specifically, gamma-ray induced scintillation light from fast electrons have a greater proportion of their scintillation light generated within the prompt component as compared to recoiled protons from neutrons.[4] The differing scintillation decay curves of three particles are shown in Fig 8.
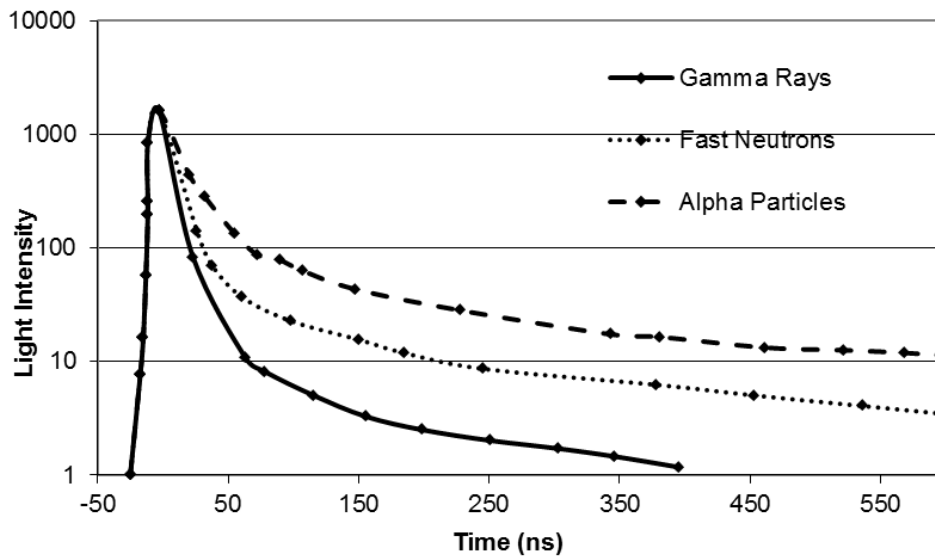
Figure 8. Time dependence of scintillation intensity for stilbene scintillator.[11]

The varying ratios of the slow component and the prompt component for fast neutrons, alpha particles, and gamma rays are due to the intensity ratio of the slow component after the ionizing event occurs. By analyzing the prompt and slow component ratios of the light pulses, it is possible to determine which ionizing particle created the light pulse. Many methods have been developed for discriminating the events, but the most common one is the charge integration method, in digital systems.

The charge integration method is where the pulse amplitude of a signal pulse is integrated over two intervals or gates. The long gate is a time interval that spans the entire pulse signal, and the short gate spans the fast component of the signal. Figure 9 is a graphic representation of the gating of a pulse signal.
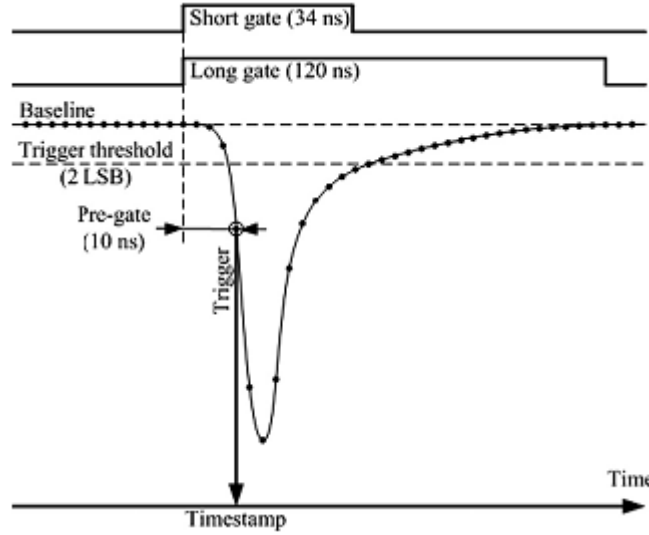
Figure 9. Representation of gating intervals in PSD.[12]

Next, the charge integrals of the long gate, Q_{long}, and the short gate, Q_{short}, are subtracted and divided by the charge of the entire pulse to calculate the PSD parameter. The PSD parameter is a measure of the ratio of the slow component's charge compared to the total collected charge.[12]

$$PSD = \frac{Q_{long} - Q_{short}}{Q_{long}}$$ Equation 2

After the PSD parameter is calculated to each pulse, identification of neutrons from gamma rays can begin.

A common method of using the PSD parameter to identify neutrons and gamma rays is to separate the particles by their PSD ratio, which can change by the detector type. Using a 2-D histogram, the limits in the PSD ratio for specific particle types can be observed. Figure 10 shows a 2-D histogram distribution of the pulses by energy output and PSD parameter with an overlay of the respective regions of neutrons and gamma rays.

19
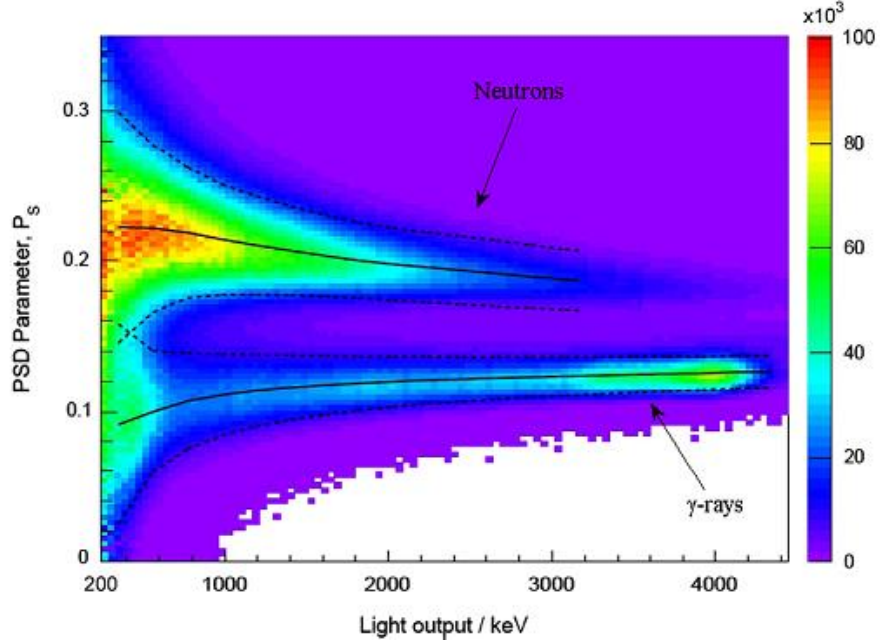
Figure 10. Two dimensional histogram of the energy versus PSD Parameter by EJ 309 measuring an AmBe source.[13]

The overlay on Fig. 10 demonstrates how low and high energy neutrons and gamma rays align and can be separated when evaluated with the PSD parameter. Then an energy filter and PSD ratio thresholds are applied to properly identify neutrons and gamma rays.

The conventional method of evaluating the reliability of PSD in a detector is analyzing the separation of the peaks of the gamma ray and neutron histogram curves. In order to do quantify the degree of separation a Figure of Merit, FOM, is calculated. The FOM is determined with the following equation:

$$FOM = \frac{P_n - P_\gamma}{\Delta P_n + \Delta P_\gamma}$$
<div align="right">Equation 3</div>

where the distance between the peaks of the neutrons, P_n, and the gamma rays, P_γ, is divided by the full-width-half-max (FWHM) of each respective curve.[13] The peaks and FWHMs are usually determined by fitting Gaussian curves to the data. EJ 309 detectors

generally have FOM of 1.8 and stilbene crystals have a FOM of 4.70.[8,14] Current research of liquid to solid neutron detectors, which are more affordable than stilbene, have a FOM of 3.31.[8]

Solidification Theory

In this work the method chosen to solidify liquid mixtures is to dissolve a scintillation mixture into a relatively inert elastomer. The material selected for this research is Polydimethylsiloxane (PDMS). PDMS is a widely used organic polymer. Its applications range from contact lenses and medical devices and to solar panel arrays. PDMS is a colorless material that has a refractive index of 1.4; water has a refractive index of 1.0 and glass's is 1.5.[15] It is inert, hydrophobic, non-toxic, and non-flammable, unlike most organic scintillators like benzene.[15] These characteristics along with the remaining in a solid state from -45 to 200 $^{\circ}$C, makes PDMS a suitable candidate for attempting to make a solid neutron detector.[15]

The chemical formula for PDMS is $(H_3C)_3SiO[Si(CH_3)_2O]nSi(CH_3)_3$, where n is the number of the repeating monomer $[SiO(CH_3)_2]$. A typical PDMS elastomer base is mixed with its curing agent in a 10:1 ratio, but it can be vary as widely as 5:1 or 33:1.[16] The curing agent for PDMS is generally a form of hydrochloric acid.[17] When the curing agent and the elastomer base are mixed, the polymerization process of cross-linking begins. Cross-linking, also known as biconjugation, is the process of chemically combining the ends of two or more molecules with a covalent bond.[18] Cross linking molecules contain at least two reactive ends that can attach to each other to form the macromolecules.[19] Heat may be applied to the elastomer mix in order to hasten the polymerization process, but crosslinking will still occur at room temperature, 25 $^{\circ}$C.[15] Macromolecules consist of multiple repetitions of molecule chains of relatively low molecular mass, such as plastics and hydro-carbon chains.[19] When the PDMS' cross-linking process is complete, then a solidified polymer is formed out of the

macromolecules.[19] With PDMS solids mixed with liquid scintillator, neutron detection

may be possible, and capabilities similar to the findings of the previously mentioned

styrene and PVT detectors mixed with other liquid scintillators.

CHAPTER 3

LIQUID EXPERIMENTAL APPROACH AND RESULTS

Liquid Mixture Selection

Before any scintillation mixtures were made a review of current liquid mixtures
was conducted for select candidate mixtures for the research. The focus of the review
was the key components of an organic scintillation mixture: solvent, primary fluor, and
wave-length shifter. The selected mixtures will be tested for neutron detection
capabilities and then developed into candidates for the solidified detectors. Reference
mixtures from Dr. Zaitseva's work and the proposed Low Energy Neutrino Astronomy
(LENA) observatory were selected after reviewing the neutron detection results of their
mixtures.[13,20] The chosen components were the solvents xylene and linear alkyl benzene
(LAB), the selected primary fluors were phenyl-mesityle-pyrazolin (PMP) and PPO, the
wave-length shifter bis-methylstyryl-benzene (MSB), and the dopant lithium oxide
additive phenyl salicylic acid (Li-3-PSA). The purchasable liquid scintillation mixture
EJ-309 was selected as a standard to compare the other mixtures to. The proposed
mixtures are in the following table.

Table 1. Proposed LS Mixtures.

Solvent/ Mixture	Primary Solute	Concentration	Secondary Solute	Conc.	Dopant	Conc.
LAB	PPO	2 g/L	MSB	20 mg/L	-	-
LAB	PMP	2 g/L	-	-	-	-
Phenyl Xylene	PPO	30% wt	MSB	0.2% wt	Li-3-PSA *	5% wt
EJ309	N/A	N/A	N/A	N/A	N/A	N/A

Once the initial mixtures were decided upon, a review of the emission spectra of the components was undertaken in order to select a PMT that matches the expected scintillation emission wavelength from the wavelength shifter. An Electron Tube 9266B PMT was selected due to its low dark noise signal and high quantum efficiency of 30% at a wavelength of 370 nm.[21] The light absorption and emission spectra of the mixture components was tabulated, shown in Table 2, to verify that the solutions matched the PMT and that the wavelength shifter, fluors, and solvents overlapped.

Table 2. Light Absorption and Emission Wavelength comparison.

Material	Absorption Spectrum Max	Emission Spectrum Max
Xylene	270 nm	290 nm
LAB	260 nm	283 nm
PPO	303 nm	365 nm
MSB	365 nm	420 nm
PMP	294 nm	415 nm
EJ 309	N/A	424 nm

After ensuring the emission wavelengths matched the PMT, supplies were gathered to make the mixtures. Two challenges were encountered while gathering materials: obtaining un-sulfonated LAB in reasonable quantities and the relatively high costs of PMP and Li-3-PSA. PMP and Li-3-PSA were deemed too expensive and were removed as components for an affordable neutron detector. The solvent LAB was removed because no vendor could be found to supply a suitable quantity for this research, because most LAB is sold by the shipping container or by drum barrels. Therefore, two final mixtures remained for testing and are listed in Table 3.

Table 3. Final LS Mixtures.

Name	Solvent/ Mixture	Primary Solute	Concentration	Secondary Solute	Conc.
Xy 1	Phenyl Xylene	PPO	2 g/L	MSB	20 mg/L
EJ	EJ309	N/A	N/A	N/A	N/A

The next step in the research was the design and purchasing of a flask to evaluate the detection characteristics of the liquid scintillation mixtures. The desired qualities for the flask are transparency, low reactivity, and precise dimensions. A quartz glass flask was selected because of its transparency, general inertness, and precision of manufacture. A flask with a neck of 53mm in inner diameter and a length of 88mm was ordered to allow the PMT's face to rest on the spherical cavity in the bulb. The bulb of the quartz flask can hold 500ml. Once the flask was received, it was wrapped in polytetrafluoroethylene (PTFE) tape for reflecting the scintillation light and then covered in electrical tape to light proof the flask from outside light. The inside of the flask was left bare.

Liquid Experimental Approach

The candidate mixtures were tested at the Radiological Science and Engineering Laboratory (RSEL) facility in the Boggs Building at the Georgia Institute of Technology. The gamma ray and neutron sources utilized for measuring the responses of the mixtures were cesium-137, sodium-22, cobalt-60, thorium-232, and plutonium-beryllium. The PuBe source is of special interest because it produces a mixed radiation field of neutrons and gamma rays. PuBe's emitted neutrons have an average energy of 3.2 MeV and the source emits 4.43 MeV gamma rays.[22]   Most non-PuBe measurements were taken in a nearby laboratory within the Boggs Building. All measurements of the PuBe source were

performed in a shielded room in the RSEL, due to the high dose rate of the source. The dose rate for the PuBe at one foot away was 23mrem/hr and outside the entrance behind a closed door it was 0.1 µrem/hr. The PuBe source was placed in a concrete box for further shielding. The equipment and software for the experiments used were an ET 9266B PMT, Canberra Model 2007 preamplifier base, Canberra DT-7730B digitizer, CAEN NDT1470 power supply, CAEN DPP-PSD software, and MATLAB software.

The initial measurements were sequential counts of Co-60 as the Xy 1 solution was mixed. The first count was only with the base solvent of xylene in the flask and the source placed directly on the midpoint of the bulb. Ten minute measurements were taken at each stage of mixing the solution as PPO, MSB, and Triton-X were added. Triton-X was added in an early version of Xy 1 in order to observe the effects of adding a surfactant, but was excluded in the rest of the mixtures. After these early measurements, gamma ray counts were conducted with the Na-22, Cs-137, Co-60, and Th-232 sources. Energy calibration for the detector was conducted with a Na-22 source. Na-22 produces two energies of gamma rays by positron emission: 0.511 MeV annihilation gamma rays and a 1.275 gamma ray. The information from these counts was used to observe the gamma ray detection characteristics of the mixtures.

The high voltage supply was set to 1000 volts and the amplifier was set for low gain runs. The signal from the PMT was routed from the anode of the amplifier to the digitizer. The amplifier and digitizer shape the signal and route it to a laptop for analysis in the DPP-PSD software.
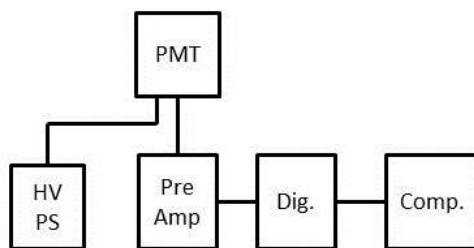
Figure 11. Diagram of data acquisition for scintillator measurements.

Figure 11 is a diagram of the entire data acquisition system. The time gating within the DPP-PSD software was set at a total gate of 128 ns.

For the PuBe measurements, a vise suspended the detector and was placed within a concrete box. The source was placed 27.2 cm away from the detector in the opposite corner. The PuBe source was located in the middle of an aluminum source holder, where the wall thickness was 3.1 cm. The space between the detector and source was used to add lead bricks, 5 cm thick each, and borated-polyethylene sheets, 2.5 cm thick each, in order to shield gamma rays and neutrons, respectively, as shown in Fig. 12.

Figure 12. Photograph of experimental setup with polyethylene shielding.

Borated polyethylene, 5% by weight, was selected for the neutron shield because boron
absorbs, instead of moderates, neutrons. Lead shielding was chosen for its high density
and large atomic number which produces a high cross section for photo electric
absorption of gamma rays of 0.5 MeV and higher energies.[4]

Liquid Experimental Results

Initial gamma ray measurements of the LS detectors were analyzed using the
energy histogram capability of CAEN's DPP-PSD software and MATLAB. Step-by-step
measurements were taken of the Xy 1 LS mixture in order to observe the effects of each
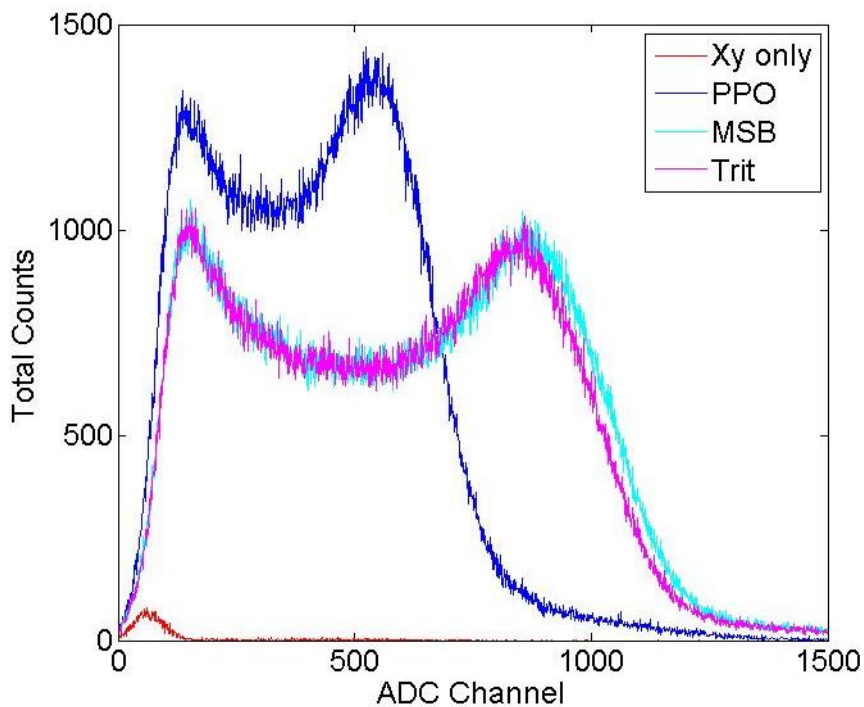component and are displayed in Fig. 13.

Figure 13. 10 minute step-by-step Co-60 energy histogram by Xy 1.

Figure 13 shows that the organic solvent Xylene is inert by itself, but a dramatic increase in responsiveness occurs when the primary fluor PPO is added. The increase occurs because the scintillation wavelength of the fluor matches the PMT. When the fluor is combined a combined gamma ray peak for Co-60's 1.17 and 1.33 MeV gamma ray emissions is formed. The addition of the wavelength shifter MSB lengthened the energy spectrum of the response by causing the LS mixture to be more sensitive to differing gamma ray energies. MSB increased the total response and energy sensitivity of the mixture; the total counts increased 6.16% . Whereas the surfactant Triton-X reduced energy sensitivity and total counts by 3.35%. Due to these results, adding surfactants to xylene mixtures was halted.

After confirming that Xy 1was responsive to gamma rays, measurements of the three other gamma ray sources Th-232, Cs-137, and Na-22 were conducted. The counts

were normalized respectfully to each source's activity and the ADC Channels were

linearly calibrated with known gamma ray energies in order to compare the energy

resolution of the gamma ray in Fig. 14.
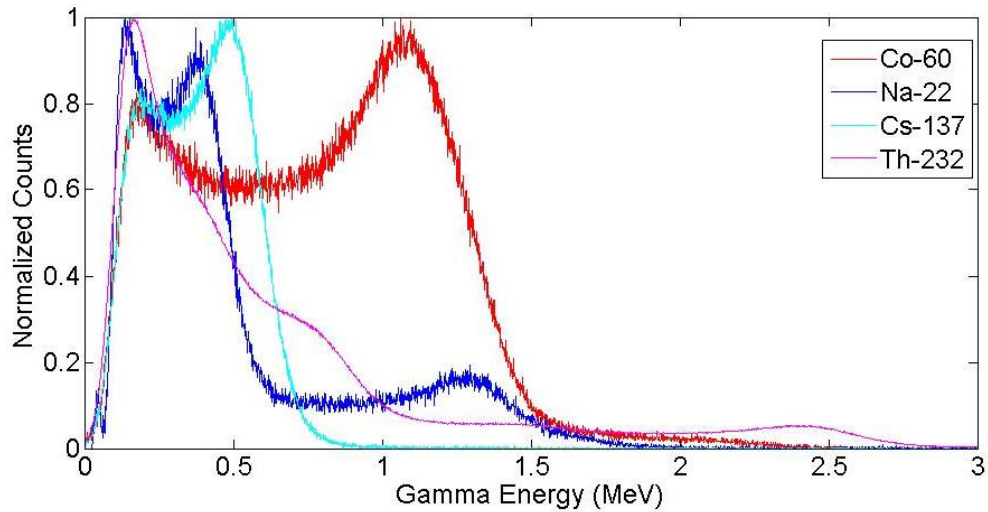
Figure 14. Calibrated and normalized energy histogram of Xy 1 measuring four sources.

In Figure 14, the Na-22 curve does not appear normalized, but at 0.33 MeV it reaches its

maximum in one channel (channel 129), but the MATLAB graphing software did not

show it. While Xy 1 is able to detect the relative energy of gamma ray edges, Xy 1 does

not have the energy resolution to separate the edges of Co-60's two gamma rays in Fig.

14.

A linear energy calibration for Xy 1, and all later organic detectors, is applied

with the measurements of Th-232's 2.617 and Cs-137's 0.661MeV gamma ray emissions

and the following method. Because the peaks forming in the histogram are the Compton

Edge of the incident gamma ray and the full energy peaks, E_o, are un-noticeable, Equation

4 is used to calculate the energy of each gamma ray's Compton Edge, E'.[4]

$$E' = E_o * \frac{2*E_o/.511}{1+(2*E_o)/.511}$$

Equation 4

The Compton Edge energies for Th-232 and Cs-137 are 2.384 MeV and .477 MeV.

Next, the midway point between the two half heights of the peaks was used to select the

channel number for the corresponding Compton Edge energy. Then a linear fit, shown in

Fig. 15, is applied between these channel numbers to convert the remaining channels into

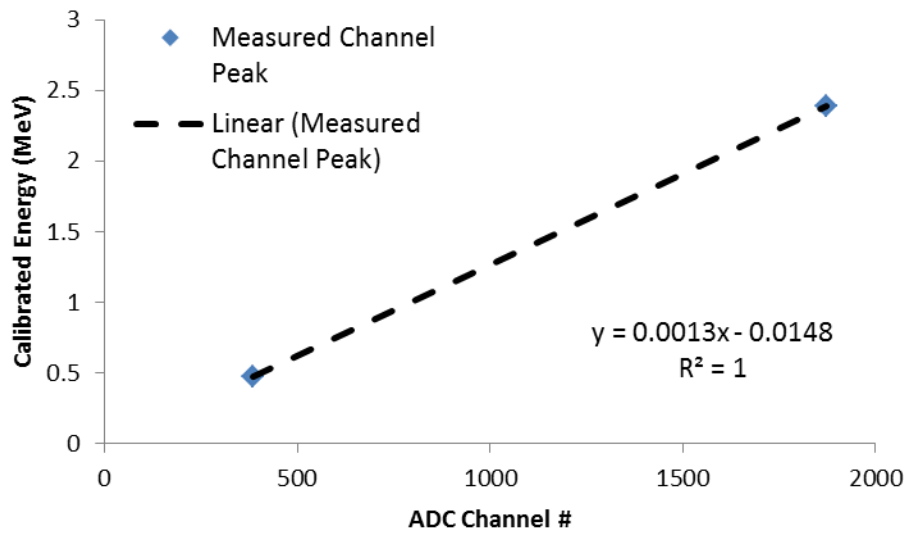specific gamma ray energies.

Figure 15. Linear energy calibration plot of Xy 1 with Th-232's and Cs-137's Compton
Edge measurements.

Using energy calibration, the energy resolution of the scintillation detector can be

assessed. The percent energy resolution, $\%_R$, is given in Eq. 5, using the FWHM and

energy of the Compton Edge.

$$\%_R = \frac{FWHM}{E'} * 100$$

<div align="right">Equation 5</div>

The energy resolution of Xy 1 for the Na-22 edge is 32.6%, which is poor compared to EJ-309 which has an energy resolution of 20.6%.[23]

  After confirming that Xy 1 was able to detect gamma rays and their respective energies, PuBe neutron measurements were initiated. Using the DPP-PSD software a series of trials were conducted in order to determine the optimal gating for Xy 1. First, a rough gating was selected while observing the pulses in oscilloscope mode by comparing the short gamma ray pulses to the longer neutron pulses. Next, 2-D histogram plots of different gatings were assessed in order to determine the optimal gating for Xy 1.
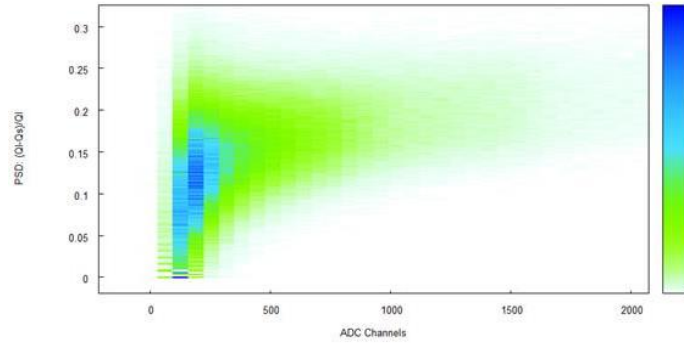
Trial 8: Short gate= 36 ns, Long gate=228 ns

(a)
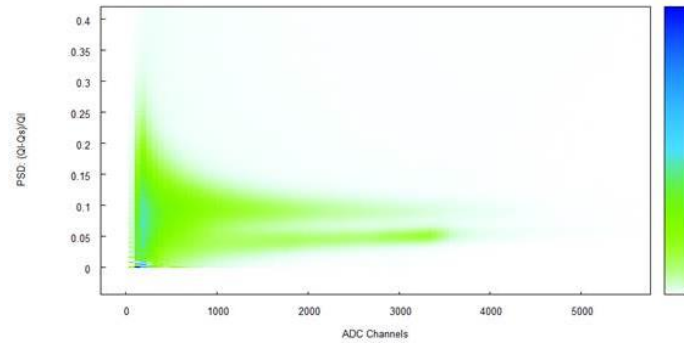
Trial 11: Short gate= 52 ns, Long gate=448 ns

(b)

Figure 16. Energy Channel vs. PSD parameter 2-D histogram comparison of liquid Xy 1's trial 8 (a) and trial 11 (b).

The trials which demonstrated a visible separation between two signals, like plot b in Fig. 16, had their respective FOM's compared to each other to find the optimal gating. Trial 3 demonstrated the greatest separation between the two curves with a long gate of 228 ns and short gate of 40 ns. With the gating established, an one hour, unshielded measurement of the PuBe was taken to determine the FOM and error of Xy 1. The FOM error, σ_{FOM}, was calculated by applying error propagation to the FOM equation, Eq. 2.[9]

$$\sigma_{FOM} = [\left(\frac{\sigma_\gamma}{FM_\gamma+FM_n}\right)^2 + \left(\frac{\sigma_n}{FM_\gamma+FM_n}\right)^2 + 2*\left(\frac{D}{FM_\gamma+FM_n}\right)^2*\left(\frac{\sigma_\gamma}{FM_\gamma+FM_n}\right)^2 + 2*$$
$$\left(\frac{D}{FM_\gamma+FM_n}\right)^2*\left(\frac{\sigma_n}{FM_\gamma+FM_n}\right)^2]^{1/2}$$

Equation 6

For Equation 6, the abbreviation FWHM has been reduced to FM, D represents the distance between the maximum peaks of the gamma ray and neutron Gaussian fitted curves. Equation 6 displays the known deviation of a Gaussian curve. [4]

$$\sigma = \frac{FWHM}{2.35}$$ Equation 7.

Utilizing MATLAB, two Gaussian curves were fitted to the date shown in the PSD histograms of Fig. 17.
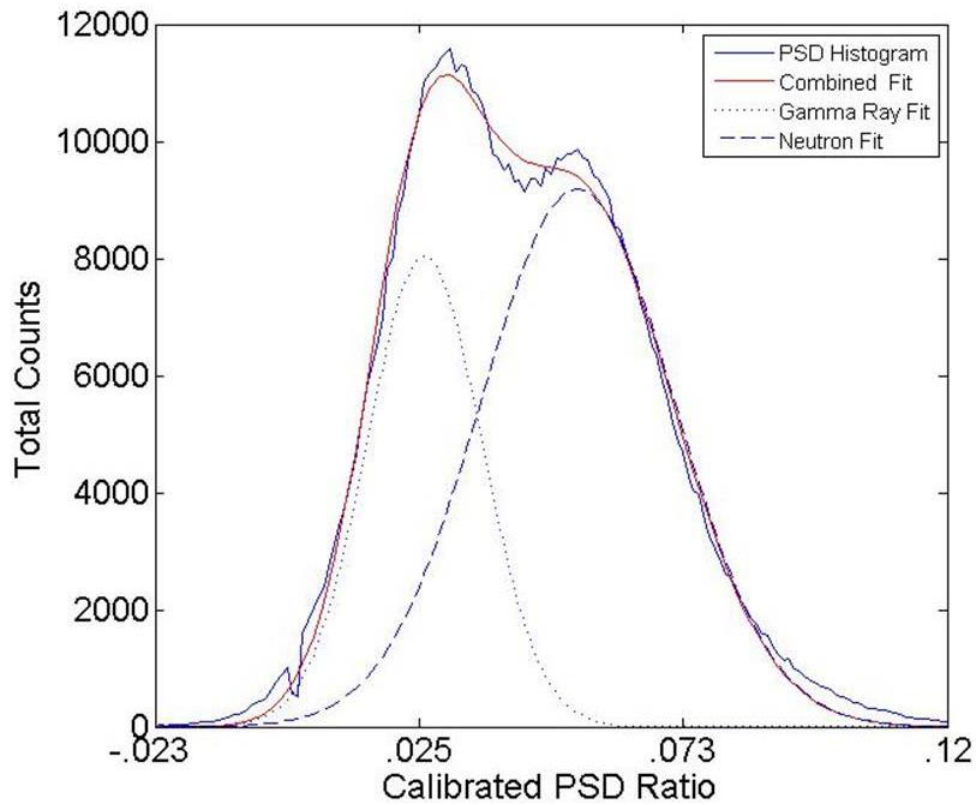

Figure 17. Calibrated PSD plot of an hour long measurement of unshielded PuBe by Xy 1 with Gaussian fits.

Additionally, the overlaid curves were assumed to be gamma rays and neutrons as seen in previous work. The FOM of Xy 1 was calculated to be 0.25 ±0.138, with the FOM and Ő$_{FOM}$ equations.

Next, the shielded measurements of PuBe was begun in order to confirm or deny whether the neutrons and gamma rays are being separated. The two visible curves shown in Fig. 17 visualize two distinct pulse signals that differ in how much of their light intensity is prompt or delayed. Previous work and theory have shown that the pulses with a higher PSD parameter, or more delayed light, are created by neutrons, and that the pulses with the lower PSD parameter are created by gamma rays. To verify that the "higher" curve is neutrons and that the "lower" curve is gamma rays, a series of measurements were taken using lead and borated polyethylene shielding.
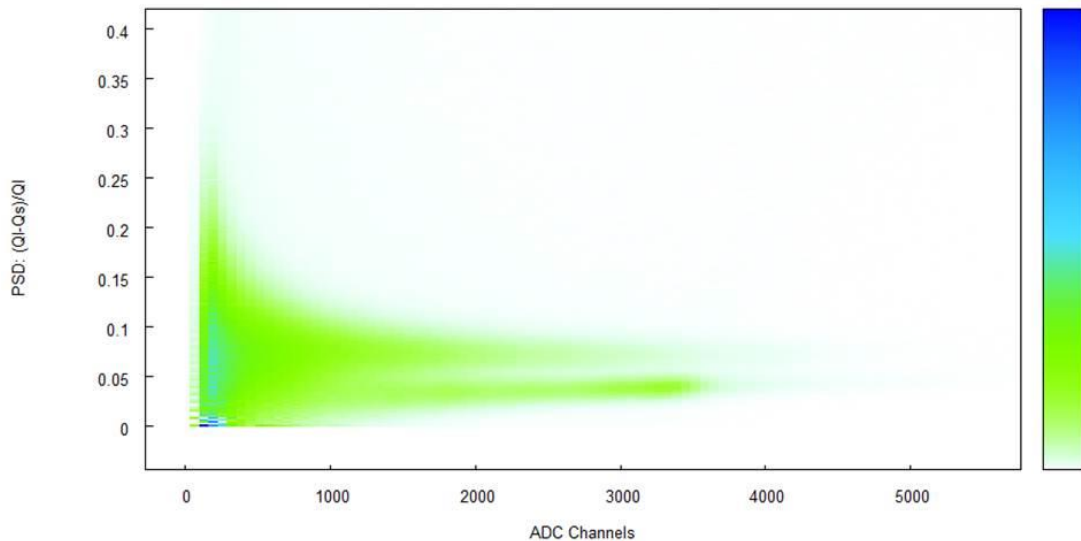
Figure 18. Xy 1 PSD plot, from DPP-PSD, of a bare PuBe source.
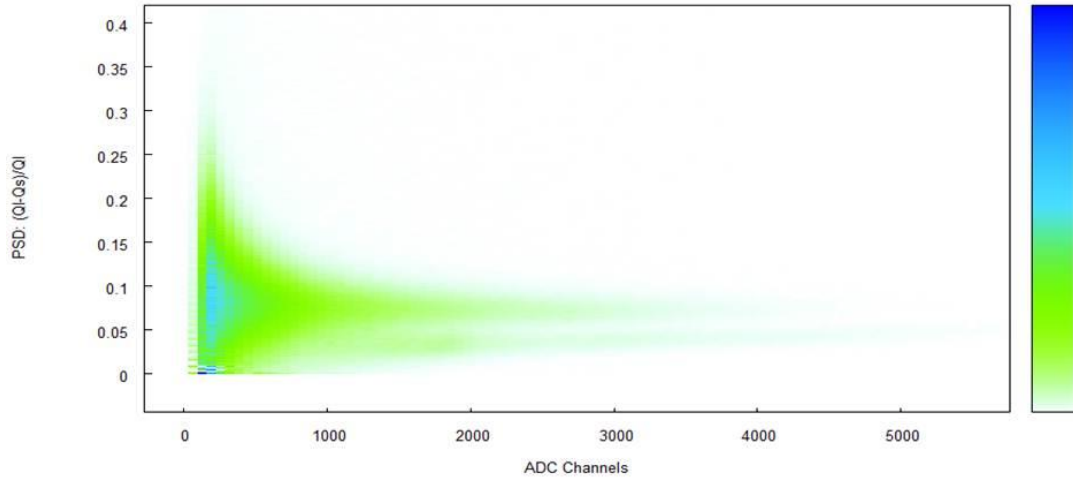
Figure 19. Xy 1 PSD plot, from DPP-PSD, of PuBe shielded with 10 cm of lead.
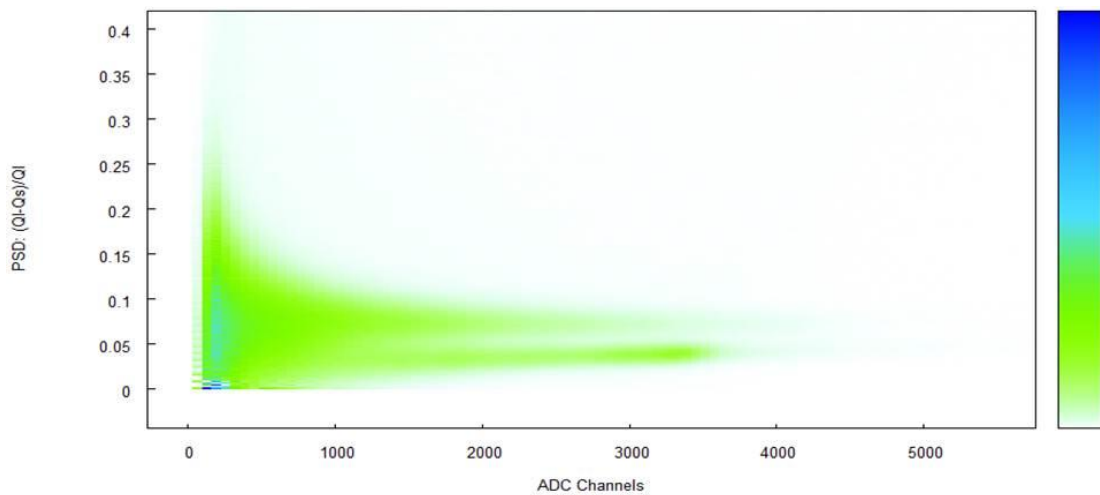
Figure 20. Xy 1 PSD plot, from DPP-PSD, of a PuBe source shielded by 5 cm of borated polyethylene shield.

The lead shielding disproportionally reduced the lower curve's high and low energy gamma rays, when comparing Fig. 18 to Fig. 19. The borated polyethylene absorbed a portion of neutron, as presented in Fig. 20. These results confirm that the two curves are not the same particle but are distinctly neutrons and gamma rays.

The confirmation of separating neutrons and gamma rays by the pulse's PSD parameter then allowed the analysis of neutrons and gamma rays without interference from the other particle. The relative minimum in the combined Gaussian fit was selected as the value of the PSD parameter for a PSD parameter filter and then applied in order to plot the energy histograms of the two particles in Fig. 21.
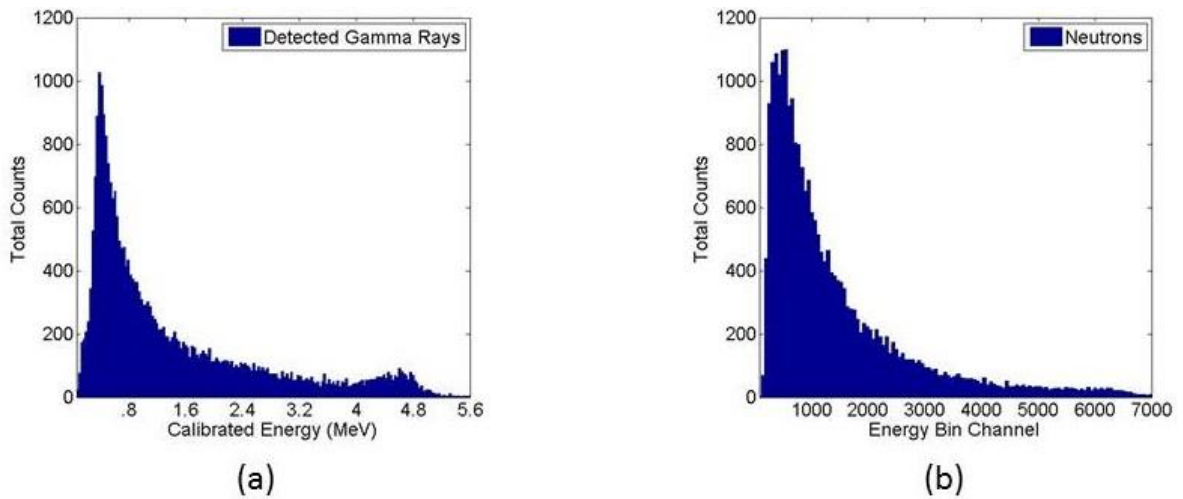
Figure 21. Energy histogram plots of Xy 1's detected gamma rays (a) and neutrons (b) separated by a PSD parameter filter.

The Compton Edge of PuBe's 4.43 MeV gamma ray is observable in Fig. 21a, but no discernable energy peaks or shoulders are observed in the neutron histogram. The gamma ray spectroscopy capability of Xy 1 is retained while being exposed to high energy neutrons.   After finalizing the measurements of PuBe, Xy 1 was replaced with EJ 309 and the next iteration of liquid experiments began.

For this round of measurements, the same four gamma ray sources and the PuBe sources were used along with the same equipment and setup. A step-by-step gamma ray

plot was not possible since EJ 309 is sold pre-made, therefore counts of the four gamma

rays sources was first.
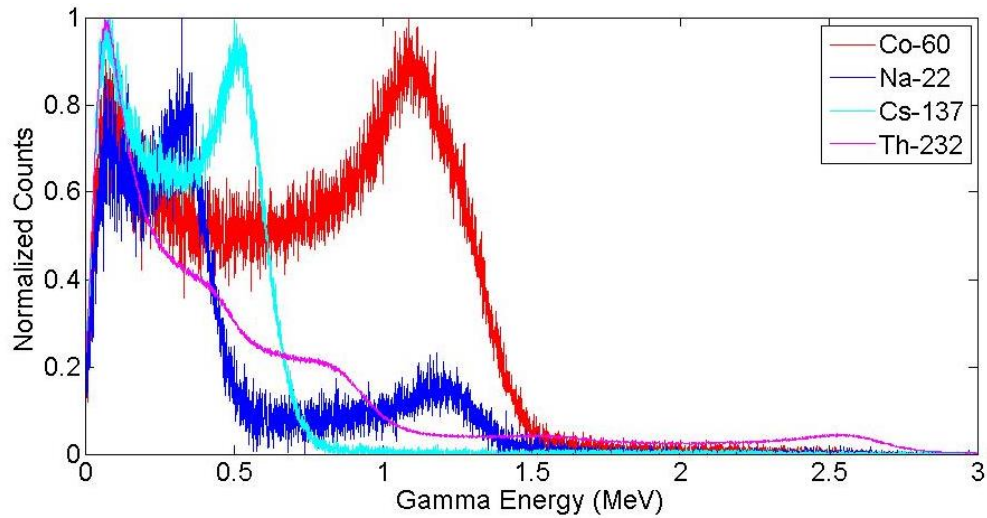
Figure 22. Normalized energy histogram of liquid EJ 309 measuring four gamma sources.

Figure 22 shows that the energy resolution of EJ 309 is slightly better than Xy 1 but the

two individual edges or peaks of Co-60 were not pronounced. Following the gamma ray

tests, PuBe PSD measurements with EJ 309 were conducted along with FOM

calculations.
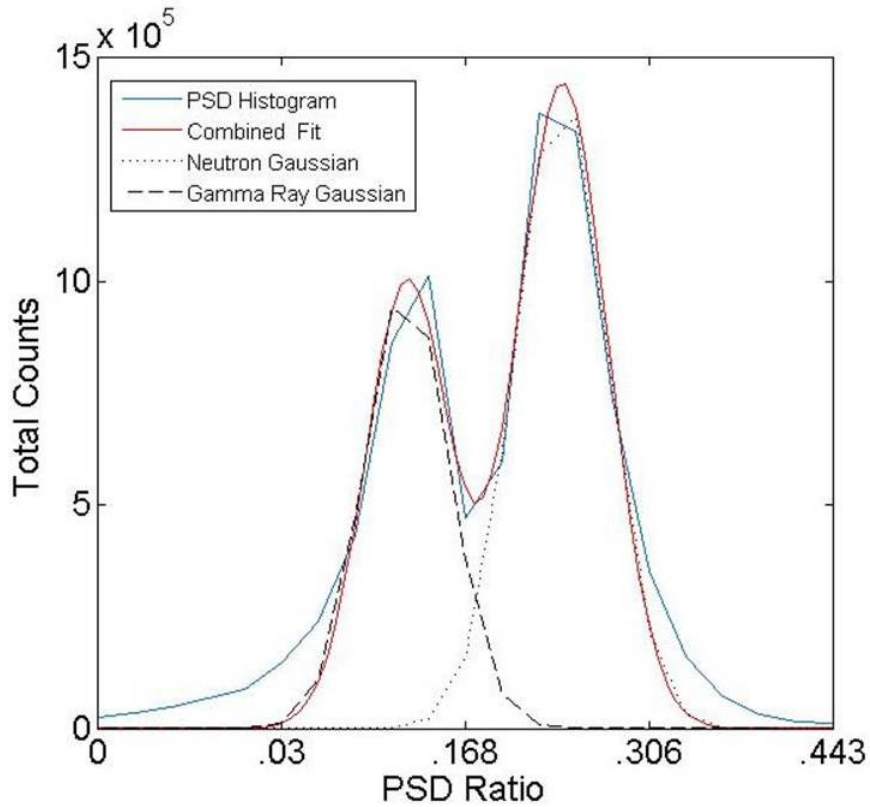
Figure 23. 1 hour PSD parameter histogram of liquid EJ 309 with Gaussian fit curves.

The FOM of the Gaussian fits from the 30 minute PuBe measurement in Fig. 23 was 0.531 ±0.188. The FOM of EJ 309 is slightly more than twice of Xy 1, which is evident in the pronounced gap observed in Fig. 23 when compared to Xy 1's separation in Fig. 17.

After defining the Gaussian PSD curves of EJ 309, a PSD parameter filter was applied to the data. Energy histograms of the detected neutrons and gamma rays were plotted in Fig. 24.
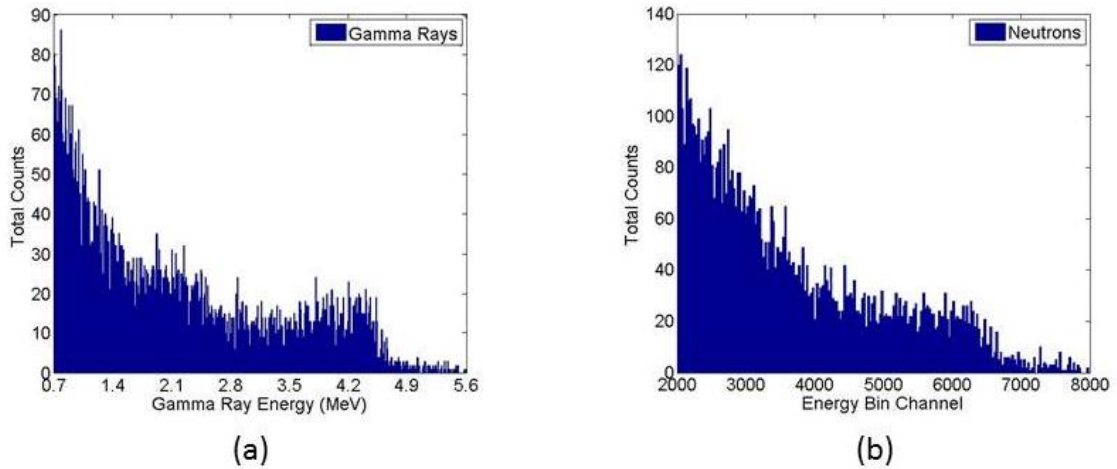
Figure 24. 1 hour EJ 309 liquid energy histogram plots of gamma rays (a) and neutrons (b) separated by a PSD parameter filter.

With a similar PSD parameter filter applied to the Xy 1 mixture, the Compton Edge for PuBe's 4.43 MeV gamma ray is observable. The ability to isolate the 4.43 MeV gamma ray's Compton Edge was expected because the edge appeared in the lower curve in the 2-D PSD histogram plot in Fig. 25.
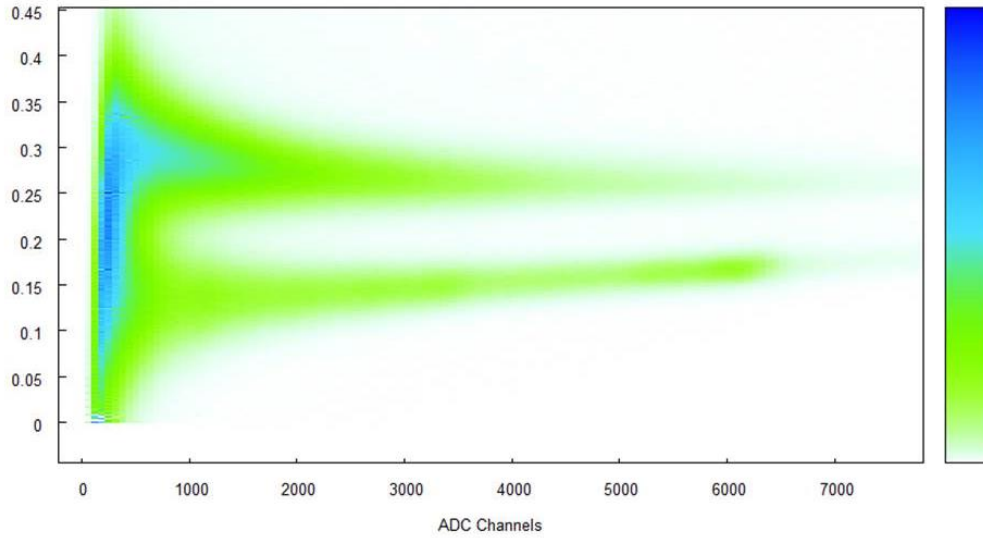
Figure 25. 2-D PSD histogram plot of a 1 hour measurement of PuBe with liquid EJ 309.

Thus, gamma ray energy spectroscopy of EJ 309 and Xy 1 are still observable in when the neutron counts are filtered out

After compiling the results of the liquid experiments, the EJ 309 LS mixture appears to be more effective at separating neutrons and clearer energy resolution. Table 4 is a summary of the results of the LS mixtures with results from a characterization study of EJ 309.

Table 4. Summary of energy resolutions and FOMs of LS mixtures and reference mixture.

Mixture	Resolution (%)	FOM	FOM Error (+/-)
Xy 1	32.64	0.25	0.138
EJ 309	20.61	0.530	0.197
EJ 309[23]	16.00	0.8	N/A

The results of EJ 309 in this work compared to another researcher's findings is promising due to the energy resolution results being similar, but the FOM results are not close.

CHAPTER 4

SOLID EXPERIMENTAL APPROACH AND RESULTS

Solidification Process

The next step in the work was the solidification of the liquid candidates. For this research, a ratio of 10:1 for the Sylgard 184 PDMS base to curing agent was selected because it is the recommended ratio from the supplier.[15] The steps utilized for making a solid sample are: mixing a 10:1 ratio of the base and curing agent, mixing the desired scintillator amount, removing air bubbles with a vacuum pump, and then cured at the desired temperature. Figure 26, below, is a visual representation of the process of mixing a LS mixture with an elastomer to make a solid detector mold.

i.	ii.	iii.	iv.
Fill Mold	Mix and Vac. Purge	Cure	Remove and Wrap
Scintillator / Elastomer / Curing Agent	Mixture	Evaporated Scintillator / Mixture	Mold

Figure 26. Solidification procedure step diagram.

Two in., five cm, diameter petri dishes were used as the container for the small 20 g samples. These samples measured approximately 0.25 cm in thickness. Plastic pipets and a mass scale were used to ensure the precision of the mixture ratios. An enclosed vacuum pump workbench pulled air bubbles that formed while mixing the scintillator and PDMS, and an incubator cured samples at temperatures above room temperature.

The curing temperatures ranging from room temperature, 25°C, to 80°C were tested to determine the optimum curing temperature. After many trials, room temperature was determined to be the optimal curing temperature due to three problems encountered with the application of heat. The three problems aggravated from higher curing temperatures were the evaporation of a significant portion of the liquid scintillator out of the mixture which degraded scintillation output, severe concave and convex faces on the molds from +90% LS evaporation that were unable to be coupled to the PMT face, and LS vapors weakening and dissolving the lid and side walls into the mold as it solidified. At room temperature the scintillation output returned and no more concave and convex faces were formed. Unfortunately, the dissolving of the petri dish into the molds at room temperature was still a persistent challenge, though less severe. Figure 27 is a picture of the organic solvents damaging a scintillating mold with its container and a later working sample.
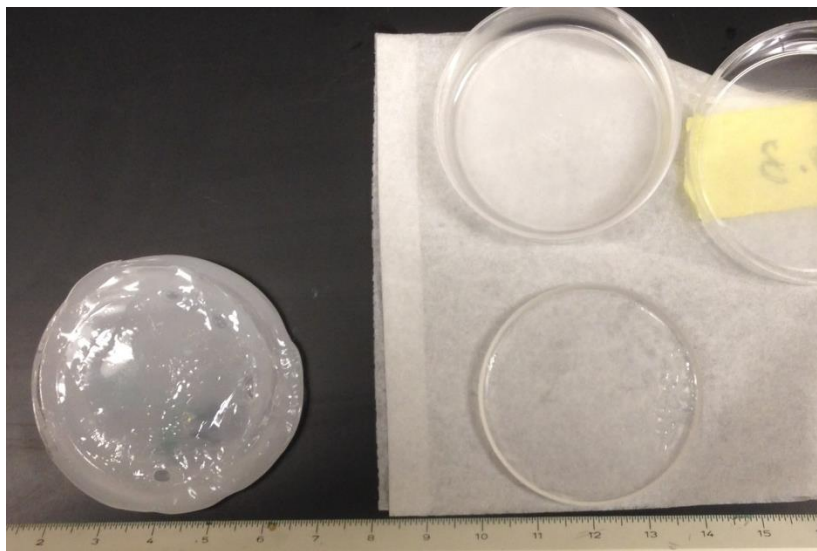

Figure 27. Photograph of a melted mold (left) and successful Xy 1 mold with cm ruler.

The persistent dissolving of the petri dishes showed that the heating of the mixtures only exacerbated the melting of the dishes and was not the cause. The solvent bases of Xy 1 and EJ 309 were suspected of being the foundation of the issue because of their organic solvent properties. After a review, it was discovered that the dishes were made of polystyrene and not the assumed polyethylene. This distinction is important because polystyrene is a plastic that is soluble in organic solvents. To correct this, two methods were selected to protect future small solid samples: aluminum foil lining or a polyacrylic acid (PAA) lining. After new samples were made with both methods, the aluminum foil method produced intact solid samples and jagged samples were extracted from dishes lined with PAA due to gaps, formed while drying, that adhered tightly to the mold. The method of lining the petri dishes with aluminum foil was chosen for producing all remaining small solid molds.

The method employed to protect the mixture as it cured focused on maintaining the optical integrity of the mold. For each mold, one piece of aluminum foil was cut, shaped, and folded in order to minimize wrinkles on the circumference of the dish and prevent the mixture from touching any polystyrene. A tight lid was then applied which pinched any wrinkles which formed. Wrinkles left "un-pinched" caused capillary action in earlier foil molds and a majority of the scintillation mixture was erroneously transferred out of the dish. The "pinching" of the aluminum foil was the last adjustment for the small sample solidification process. Table 5 is a summary of the small Xy 1 samples highlighting their main corrective action, curing outcome, and LS:PDMS ratio.

Table 5. Summary of Xy 1 small samples.

Name	Production Date	LS:PDMS Ratio	Result	Corrective Action
1	6-Oct-15	50/50	Melted	Use room temp
2	6-Oct-15	25/75	Melted	60 C
3	6-Oct-15	15/85	Cured	Increase LS ratio
1 remake	13-Oct-15	50/50	Melted	Aluminum foil
2 remake	13-Oct-15	25/75	Melted	PAA liner
4	13-Oct-15	25/75	Partial cure	PAA liner
2 remake	28-Oct-15	25/75	Cured	Refine aluminum liner
2 remake	1-Nov-15	25/75	Cured	Enlargen sample
1 remake	9-Nov	50/50	Partial cure	Stopped 50/50 ratio
2 Larger	13-Nov-15	25/75	Partial cure	Reduce capillary action
2 Larger	17-Nov-15	25/75	Cured	Ordered larger dish

PDMS and EJ 309 samples were created once the production process was refined. After the small solid sample production was refined the next step was to apply the working process on larger samples. For creating larger samples, the polystyrene dishes were replaced PTFE dishes were chosen for their known and verified inactivity with benzene and xylene.

The larger samples were produced in 3.5 in. wide, 250 mL PTFE dishes. The same solidification process was used except for using an aluminum liner. The aluminum liner was unnecessary due to PTFE being insoluble in the organic solvents. Three large samples were made: two EJ 309 molds and a Xy 1 mold. The first EJ 309 mold was rendered un-usable by a chemical reaction between the PDMS and EJ 309 where the reaction clouded the mixture and made the mold opaque. The reaction between the two solutions is unknown due to the recipe for EJ 309 not being published. This was unexpected because the ratio of EJ 309 to PDMS, 25%/75%, was used in earlier small

samples which did not experience this issue. The next EJ 309 sample reduced the EJ 309 content from 25% to 6.25% of the whole mixture and successfully cured into a useable mold. The large Xy 1 mold was unusable due to 79.4% of the LS evaporating out of the mixture before solidification.

Finally, a cost analysis of the detectors was completed for assessing the feasibility of fielding the solidified detectors and comparing them to currently available detectors. The material cost of each mixture component of the detector was utilized to determine the cost of each mold. The total cost was divided by the final mass of the detector. Shipping costs and taxes were not included. The results of this method depict the material costs of the final mold in Table 6.

Table 6. Cost comparison of solidified detectors.

Detector	Cost per gram ($/g)
EJ 309 (small)	$ 0.179
EJ 309 (large)	$ 0.127
Xy 1 (small)	$ 0.133
Stilbene (vendor)	$ 64.357
EJ 309 (vendor)	$ 0.255

Solid Experimental Approach

A similar experimental approach of the liquid detectors was replicated for the solid detectors. The same equipment was used except for the large EJ 309 mold, where a

larger PMT was utilized. A RCA 8054 PMT was selected for the large 3.5 in mold. The switch was made because the large molds were difficult to properly wrap for a 2 in. PMT face. The 3 in. face of the RCA 8054 assisted by significantly reducing the exposed surface area of the mold coupled to the PMT face. The smaller amount of exposed surface area on the underside of the mold eased the application of PTFE reflective tape. The applied voltage was increased from 1000 V to 1800 V for the large mold and RCA 8054 PMT. The RCA 8054 has a quantum efficiency of 18% at 440 nm.[24] The last change was placing the gamma ray sources directly on top of the origin of the circular mold, instead of on the flask's midpoint. For the PuBe measurements, the geometry was maintained precisely between the liquid and solid experiments.

Solid Sample Results

The successful molds were wrapped with PTFE and light proofed before the measurements were taken. The initial measurements of all small molds were with the same four gamma ray sources of Na-22, Cs-137, Co-60, and Th-232. The results differed from the LS detectors in which shoulders were formed instead of clear gamma ray Compton edges. Since gamma ray edges did not form for the small molds, energy calibration of their ADC channels was not performed.
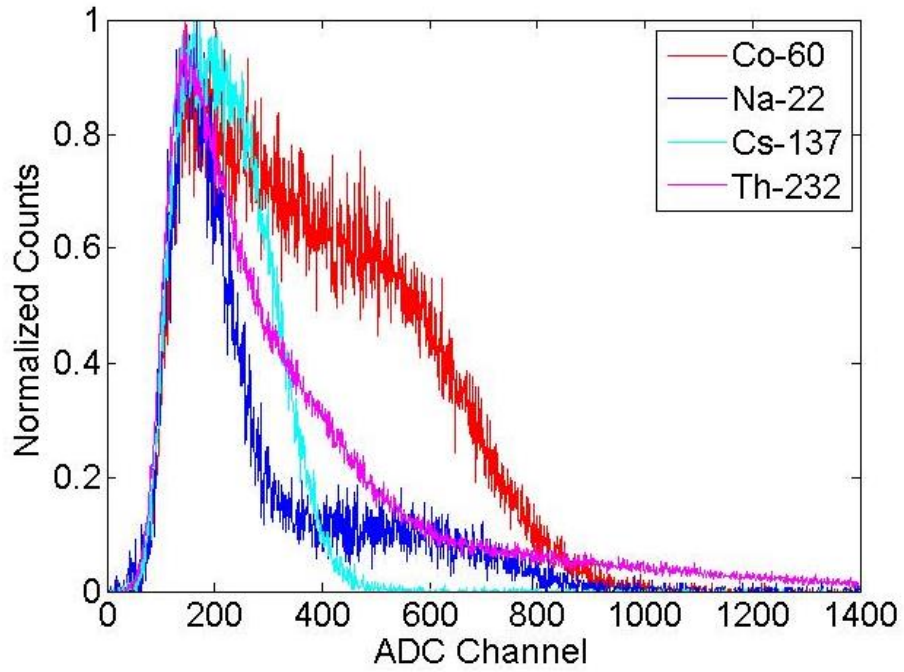
Figure 28. Normalized four source plot of small solid Xy 1 mold.
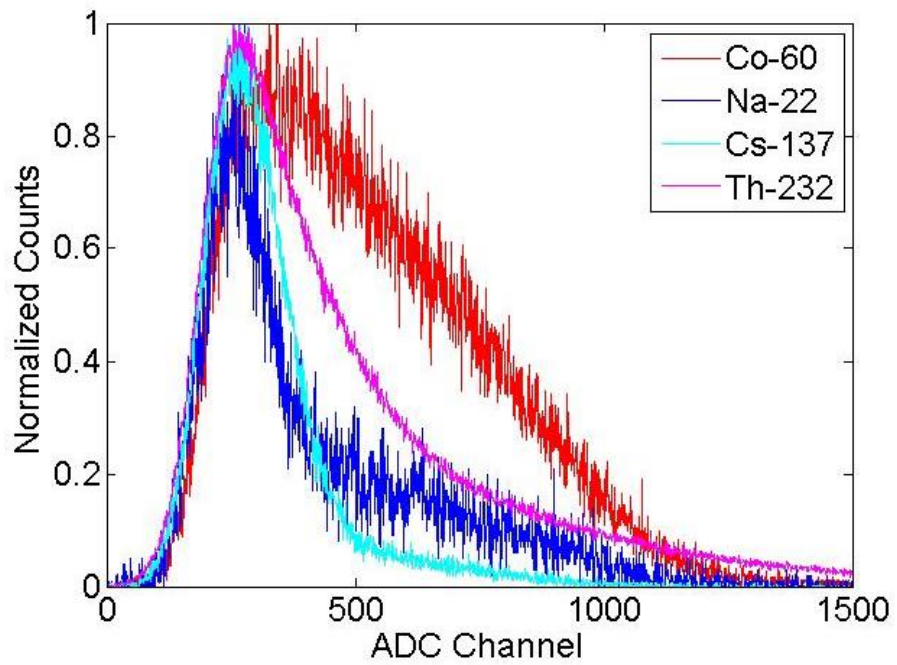

Figure 29. Normalized four source plot of small solid EJ 309 mold.

The results of the small EJ309 and Xy 1 molds in Figs. 28 and 29 are similar, but the large EJ 309 mold was different. The large EJ 309 mold began to form edges after clearing a 0.5 MeV threshold. A rough energy calibration was performed on the combined 1.25 MeV edge of Co-60 and the 0.667 edge of Cs-137 and applied to Fig. 30b.
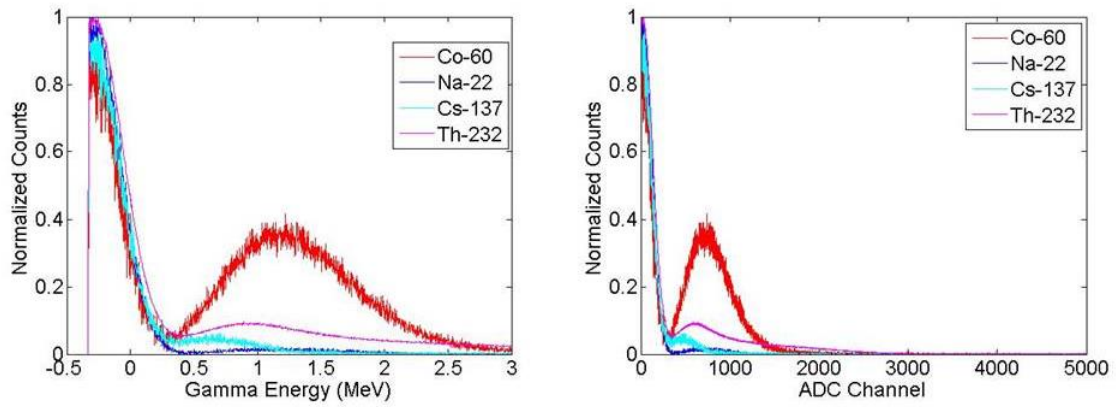

Figure 30. Uncalibrated four source plot of large solid EJ 309 mold (a) and calibrated four source plot (b).

The energy calibration of the large EJ 309 detector is not to be relied upon, because many of the low energy counts and dark noise was converted into negative gamma ray energy counts. In addition, a pure PDMS mold was formed in order to confirm or deny the interference in the signal created in the solid detectors. The PDMS only mold was exposed to the same gamma source and geometry.
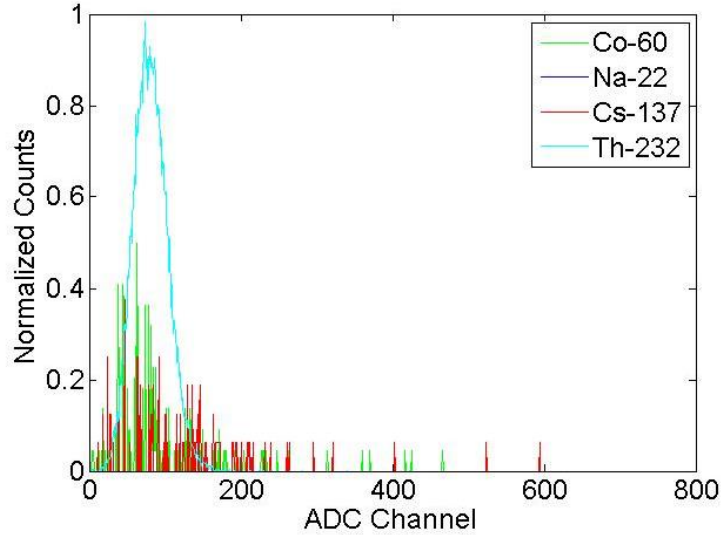
Figure 31. Normalized four source plot of a PDMS only.

In Figure 31, the background was included in the count normalization in order to observe the source created signal compared to the background. While the Th-232 source showed a sizable signal compared to the background with the PDMS only solid detector, this signal is still relatively small compared to the responses of the Xy 1 and EJ 309 molds. The PDMS mold measurements demonstrate that the Xy 1 and EJ 309 molds are not notably affected by their PDMS component.

Once the gamma ray measurements were complete, the PuBe PSD measurements were conducted.   The initial PuBe measurements with the molds did not form two distinct PSD parameter curves. Instead, a large low energy signal dominated the base of the 2-D plot, but two faint high energy Gaussian curves were noticeable. In Figure 32, a 2-D PSD histogram is displayed with a super imposed line marking the boundary between the two curves.
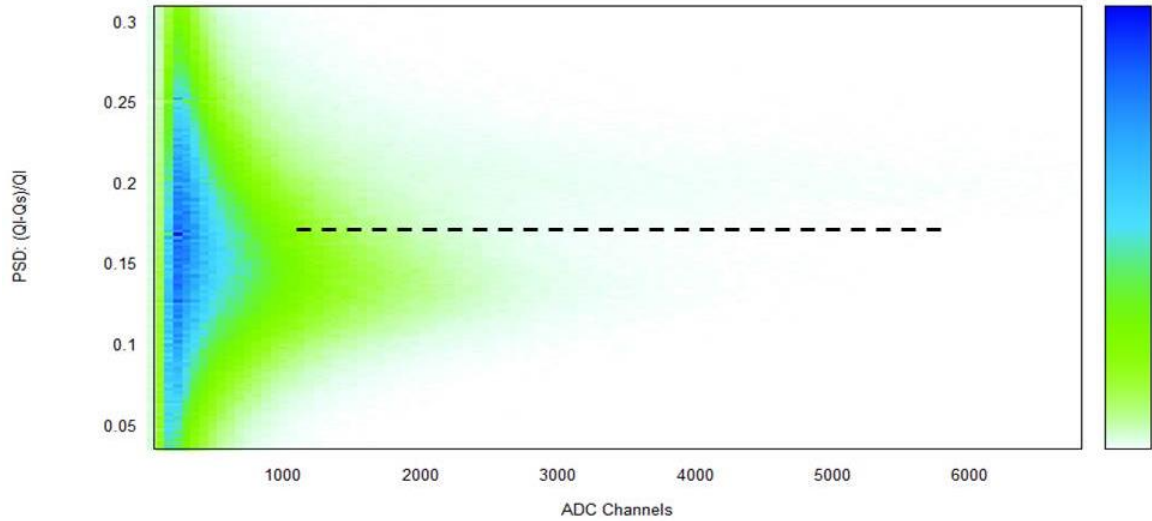
Figure 32. A one hour DPP-PSD 2-D plot measurement of the PuBe source by the small EJ 309 mold.

A series of increasing energy filters was applied upon the data to remove the noise of the low energy signal and uncover the Gaussian curves for the neutron and gamma ray signals. An energy filter of Q_{long}, or the total charge collected within the long gate of the pulse, was selected in order to focus on the total energy of the signal and not the prompt charge collected within the short gate. Figure 33 illustrates the change in the PSD parameter histogram plot as the lower energy signals are filtered out and the two signal curves emerge.

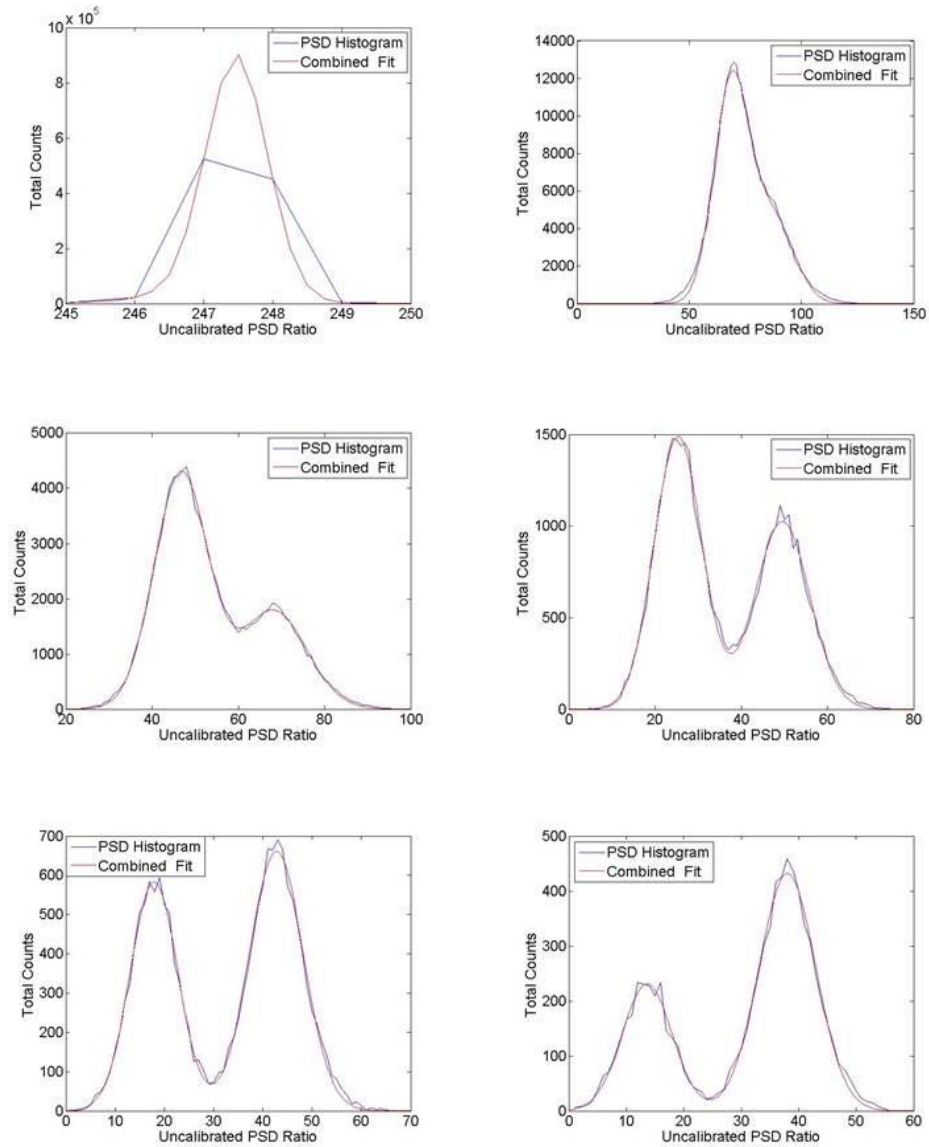Figure 33. Series of PSD parameter histograms as the energy filter is increased to separate high energy neutrons and gamma rays in the small EJ 309 mold.

With a functioning energy filter which uncovers the gamma ray and neutron curves, shielded measurements of the PuBe are begun in order to verify the separation of gamma rays and neutrons. In Figure 34, an energy filter of Q_{long} 2400 is applied to

measurements of a PuBe source with no shield, 7.5 cm of borated polyethylene shielding, and 10 cm of lead shielding.
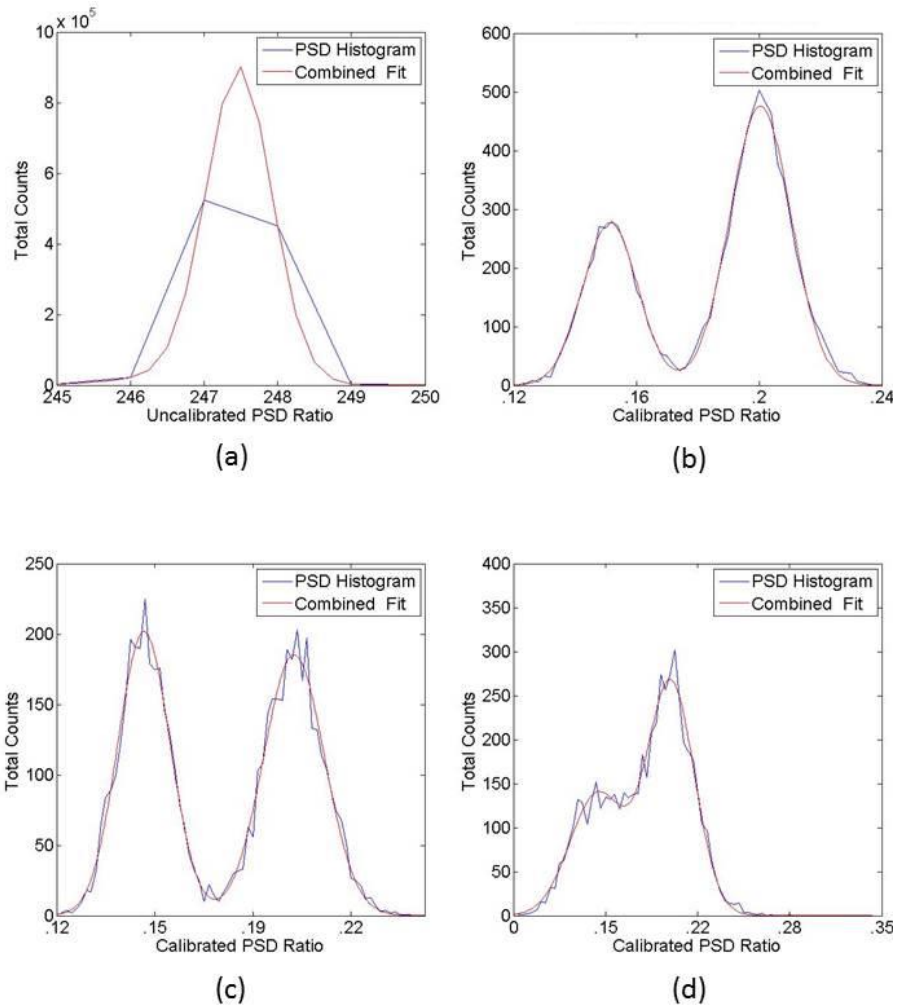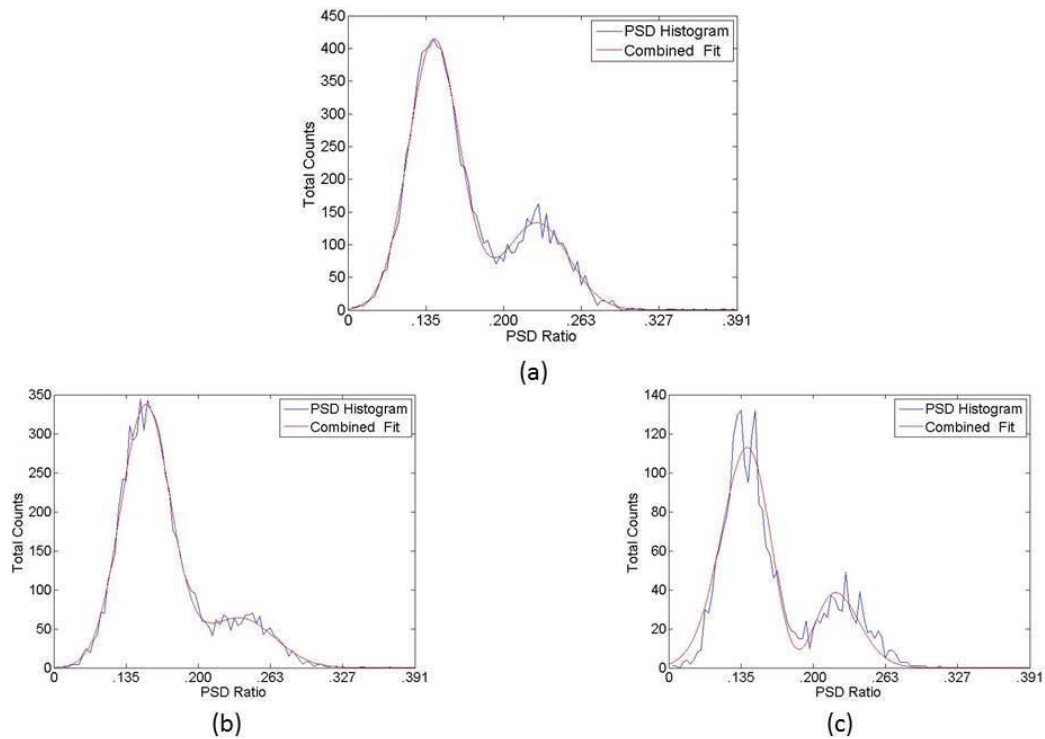

Figure 34. Comparison of the small EJ 309 mold PSD histograms with different shielding during one hour counts: unfiltered and bare (a), filtered and bare (b), filtered with 7.5 cm of poly shielding (c), filtered with 10 cm lead shielding (d).

Figure 34c illustrates a large drop in counts for the curve on the right with polyethylene shielding and Fig. 34d shows a large decrease in the counts of the left curve, when compared to the unshielded source in Fig. 34b. The disproportionate reductions in counts of the EJ 309 mold by shielding parallels the results of shielding Xy 1 with lead and borated polyethylene, in Figs. 18-20. The observed reductions of separated signals in Fig. 34 confirm that the two signal curves are gamma rays and neutrons. Occasionally an energy filter uncovered the Gaussian signal curves with the bare source but not with the lead shielded PuBe source. Increasing the threshold of the Q_{long} filter corrected this. Figure 35 illustrates the same effect polyethylene and lead shielding has upon the large EJ 309 mold.

Figures 35. Comparison of the large EJ 309 mold PSD histograms with different shielding during two hour counts: bare (a), 7.5 cm of poly (b), 15 cm of lead (c).

With the verification of gamma ray and neutron separation with the shielded measurements, the FOM of the solids was determined with the energy filter. Figure 36 is a plot of the FOM of the three solid detectors as a function of the filter's Q_{long} setting.
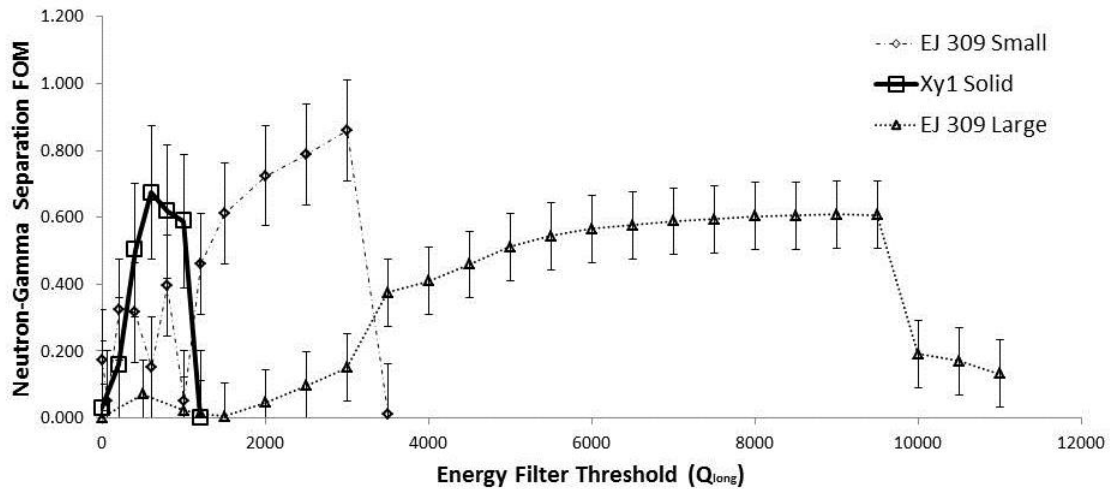

Figure 36. Energy filter threshold vs. Unshielded FOM plot.

Every solid's FOM generally increases to a maximum as the threshold of the energy filter is increased. The FOM then reaches a peak and subsequently falls to zero. The FOM "function" initially rises in all cases because the filter is reducing the inseparable low energy noise and signals and leaves the separable high energy signals. Eventually, the FOM calculation drastically drops as the entire gamma ray curve is reduced and only the neutron Gaussian curve is left. This response is expected because PuBe emits 4.43 MeV gamma rays, but also emits 8 and 10 MeV neutrons that are still detected by the molds.[22] The energy filter is not calibrated because the measurements with the molds did not yield discernable edges and each mold's response was not the same to each energy. If each

solid detector is able to calibrated, then their respective FOM calculations can be compared by gamma ray energy.

After refining the PSD of the molds, the PSD parameter filter was applied to the data and an energy histogram was plotted.
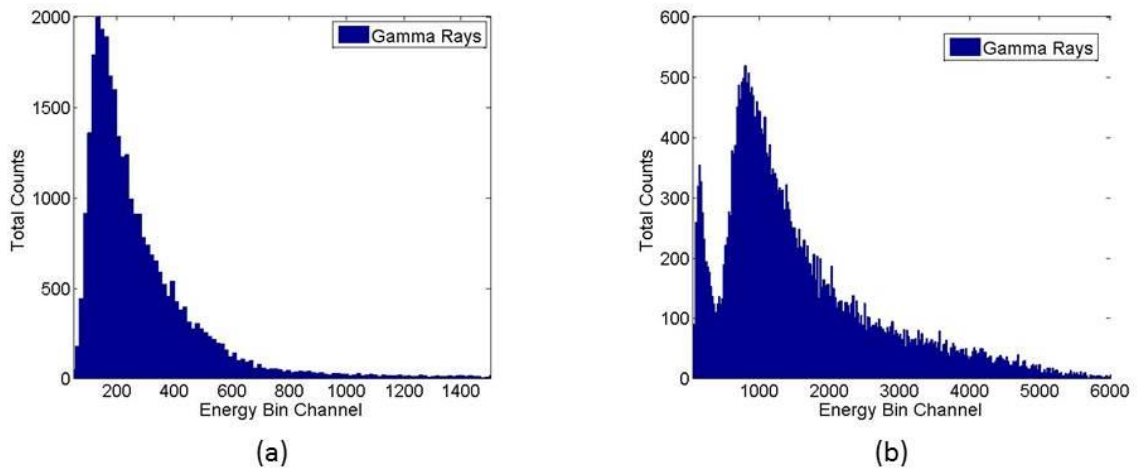
Figure 37. Gamma ray energy histograms of PuBe with Xy 1 (a) and large EJ 309 (b) molds.

Unfortunately, the 4.43 MeV gamma ray Compton Edge of PuBe did not form in any of the molds as shown in Fig. 37. This was expected because only shoulders formed for the solid detectors from the pure gamma source measurements.

The results of the solid detectors are promising for future neutron detectors when compared to their previous liquid performance. The solid detectors are hydrophobic, less flammable, and separate neutrons from gamma rays, but their energy resolution was greatly reduced. Surprisingly, the small EJ 309 mold had the greatest separation of between the neutron and gamma ray curves, shown in Table 7.

Table 7. FOM summary of solid molds.

LS Mixture	Volume (cm^3)	LS Ratio %	Initial mass (g)	Cured mass (g)	Peak Unshielded FOM	FOM Error (+/-)	Duration of FOM Run (hr)
Xy 1 (small)	8.11	25	20.00	18.00	0.673	0.214	3
EJ 309 (small)	8.11	25	16.27	13.63	0.859	0.419	1
EJ 309 (large)	99.31	6.25	93.50	93.27	0.608	0.196	2
PDMS (only)	8.11	0	8.03	7.02	N/A	N/A	N/A

The large EJ 309 mold had the lowest degree of separation of the curves and this might be due to the PMT face not covering the entire surface area of the its mold and the reduced LS ratio.

CHAPTER 5

CONCLUSION AND FUTURE WORK

Conclusion

In this work, solidified organic scintillator detection systems accurately performed PSD in order to separate neutrons and gamma rays. MATLAB software was implemented to separate the signals with an applied energy filter. Measurements of Co-60, Na-22, Cs-137, and Th-232 were conducted to confirm gamma ray detection before proceeding to neutron detection. The performances of the systems were verified by measurements of unmoderated PuBe, lead shielded PuBe, and borated polyethylene PuBe. The goal of this thesis work was to produce a working neutron detector usable in a field environment from LS mixtures. The goal was achieved by the small and large EJ 309 solidified detectors. These detectors can be placed into a mixed radiation field and detect high energy neutrons. These results are encouraging but more work needs to be done.

Future Work

This work has not completed the research necessary for developing a cheap and durable neutron detector. The following may assist in the development of neutron detectors or aid in the methods of development:

- Other LS mixtures should be explored, especially LAB and solvents other than xylene.
- An automated system or code of establishing energy filters for solidified detectors will expedite the testing other molds and mixtures.
- Constructing a LS system which can produce improved energy resolution of gamma rays and neutrons will assist in assessing the effectiveness of test LS solutions.

- Automation of finding optimum energy filter for the large solid detectors

- Experiments to determine the cause of EJ 309 reacting with Sylgard 184 in order to increase the percentage of EJ 309 in the mold.

REFERENCES

[1] U.S Government, Nuclear Regulatory Commission. "Special Nuclear Material." www.nrc.gov/materials/sp-nucmaterials.html

[2] U.S Government, Department of Energy. *Science-Based Nuclear Security and the Iran Agreement.* DoE, 31 Aug. 2015

[3] Wurm, Michael. *The Next-generation Liquid-scintillator Neutrino Observatory LENA*. Astroparticle Physics, 35, 685-732 (2012).

[4] Knoll, Glenn. Radiation Detection and Measurement. 3rd edition (2000).

[5] Simko, Thomas, and Matthew Gray. *Lunar Helium-3 Fuel for Nuclear Fusion Technology, Economics, and Resources.* World Future Review, 6.2, 158-171 (2014).

[6] Adee, Sally. "Physics Projects Deflate for Lack of Helium-3: U.S. radiation detectors suck up the existing supply." IEEE Spectrum (2010). http://spectrum.ieee.org/biomedical/diagnostics/physics-projects-deflate-for-lack-of-helium3

[7] Birks, John. The Theory and Practice and Scintillation Counting. 2nd edition (1964).

[8] Zaitseva, Natalia. *Plastic Scintillators with Efficient Neutron/gamma Pulse Shape Discrimination*. Nuc. Instr. Meth., 668, 88-93 (2012).

[9] Blanc, Pauline. *Neutron/gamma pulse shape discrimination in plastic scintillators: Preparation and characterization of various compositions.* Nuc. Instr. Meth., 750, 1-11 (2014).

[10] Saylor Academy. "Introductory Chemistry." https://saylordotorg.github.io/text_introductory-chemistry/s20-organic-chemistry.html

[11] Bollinger, L., Thomas, G., *Measurement of the Time Dependence of Scintillation Intensity by a Delayed Coincidence Method*. Rev. Sci. Instrum. 32, 1044 (1961).

[12] CAEN. *DPP-PSD: User Manual UM2580*. CAEN SpA (2015).

[13] Tomanin, A. *Characterization of a cubic EJ-309 liquid scintillator detector.* Nuc. Instr. Meth., 756, 45-54 (2014).

[14] Gerling, Mark. *Comparison of Stilbene neutron detection performance to EJ-309.* Sandia National Laboratory (2014).

[15]   Dow Corning. *Sylgard 184 Silicone Elastomer*. Datasheet (2014).

[16]   Wang, Zhixin. Polydimethylsiloxane Mechanical Properties Measured by Macroscopic Compression and Nanoindentation Techniques. Scholar Commons University of South Florida (2011).

[17]   Wikipedia. "PDMS." http://en.wikipedia.org/wiki/Polydimethylsiloxane

[18]   ThermoFisher Scientific. "Chemistry of Crosslinking." https://www.thermofisher.com/us/en/home/life-science/protein-biology/protein-biology-learning-center/protein-biology-resource-library/pierce-protein-methods/chemistry-crosslinking.html

[19]   Jenkins, A.D., Kratochvil, P. Glossary of Basic Terms in Polymer Science. International Union of Pure and Applied Chemistry, 68, 2287-2311 (1996).

[20]   Saylor Academy. "Introductory Chemistry." https://saylordotorg.github.io/text_introductory-chemistry/s20-organic-chemistry.html

[21]   ET Enterprises. 9266B series data sheet. Data sheet (2010).

[22]   *RSEL Orientation: Radiation Sources and Instruments.* Georgia Institute of Technology (2015).

[23]   Bourne, Mark M. *Measurement of Detector Resolution for Neutral Particle Detection with Liquid Scintillators.* Nuclear Science Symposium Conference Record (2010).

[24]   Radio Corporation of America. Photomultiplier Tubes: 8053, 8054, 8055. Datasheet (1967).